Chebyshev approach to quantum systems coupled to a bath

Andreas Alvermann and Holger Fehske
Institut für Physik, Ernst-Moritz-Arndt-Universität Greifswald, 17489 Greifswald, Germany
(Received 22 September 2007; published 18 January 2008)

We propose an alternative concept for the dynamics of a quantum bath, the Chebyshev space, and a method based on this concept, the Chebyshev space method. The Chebyshev space is an abstract vector space that exactly represents the fermionic or bosonic bath degrees of freedom, without a discretization of the bath density of states. Relying on Chebyshev expansions, the Chebyshev space representation of a bath has very favorable properties with respect to extremely precise and efficient calculations of ground state properties, static and dynamical correlations, and time evolution for a great variety of quantum systems. The aim of the present work is to introduce the Chebyshev space in detail and to demonstrate the capabilities of the Chebyshev space method. Although the central idea is derived in full generality, the focus is on model systems coupled to fermionic baths. In particular, we address quantum impurity problems, such as an impurity in a host or a bosonic impurity with a static barrier, and the motion of a wave packet on a chain coupled to leads. For the bosonic impurity, the phase transition from a delocalized electron to a localized polaron in arbitrary dimension is detected. For the wave packet on a chain, we show how the Chebyshev space method implements different boundary conditions, including transparent boundary conditions replacing infinite leads. Furthermore, the self-consistent solution of the Holstein model in infinite dimension is calculated. With the examples, we demonstrate how highly accurate results for system energies, correlation and spectral functions, and time dependence of observables are obtained with modest computational effort.

DOI: 10.1103/PhysRevB.77.045125 PACS number(s): 02.70.Hm, 71.27.+a, 73.21.−b, 71.38.−k

I. INTRODUCTION

The calculation of spectral or dynamical properties of quantum systems, expressed through spectral functions or captured in the time evolution of a wave function, is one of the most important and most promising applications of modern numerical techniques in theoretical physics or chemistry. For many purposes, approximation free techniques that allow to calculate numerically exact results for arbitrary Hamiltonians on large Hilbert spaces are of interest. One of the most powerful tools in this context are techniques based on Chebyshev expansions, such as the kernel polynomial method (KPM),[1–5] which yield results of high accuracy with modest computational effort. Chebyshev techniques often outperform the Lanczos algorithm with respect to accuracy and efficiency, and are applicable to problems that are beyond the reach of matrix diagonalization. In this paper, we propose an extension of Chebyshev techniques that considerably enlarges their field of applications. Possible applications we have in mind include (i) damping and decoherence in quantum systems coupled to an environment such as a bosonic heat bath, (ii) transport through quantum systems coupled to fermionic baths, (iii) the solution of quantum impurity models, (iv) nonequilibrium dynamics of mesoscopic devices coupled to leads, and in general, (v) the calculation of static and dynamical correlation functions or time propagation in these physical situations, (vi) the combination with diagrammatic Green function techniques, and (vii) the treatment of degrees of freedom with nontrivial dynamics such as phonons with dispersion.

We concentrate here on a situation for which the development of ideas is particularly clear: A quantum system coupled to a fermionic bath. The bath serves as a reservoir for fermions, which can hop from the bath to the quantum system and back. The standard example is that of a mesoscopic system contacted with leads.[6,7] For a single quantum dot, the appropriate model is the famous Anderson model for the Kondo effect,[8] which describes an impurity site with Coulomb interaction embedded in a host of noninteracting electrons. This model also arises in dynamical mean-field theory (DMFT) where the solution of an Anderson model in dependence on a host spectral function is a central issue.[9]

In all these cases, the quantum system allows for many-particle interactions, which give rise to nontrivial correlations. For their description, one has to rely on several correlation functions whose calculation requires the full apparatus of many-body theory. In the numerical calculation, we have to deal with complicated objects such as a Fock space of many fermions. Due to the coupling between the quantum system and the bath, further correlations between the quantum system and the bath develop. As a consequence, one cannot separate the degrees of freedom of the quantum system and of the bath, but must treat their evolution in parallel. However, the bath consists of noninteracting fermions, and is entirely described by single-particle spectral functions, as no correlations exist in the absence of coupling to the quantum system. Plainly spoken, we do not need to describe all details of the bath, but only how its presence influences the dynamics of the quantum system. It is important to exploit this simplification to make a calculation possible. Trivial as this point may seem, it is not easily incorporated into a numerical calculation. The numerically exact techniques to which Chebyshev techniques belong require an explicit representation of the bath degrees of freedom in terms of a Hamiltonian and an associated Hilbert space. In the worst case, such a representation again involves a many-body Fock space, describing the bath with the same complexity as the interacting quantum system.

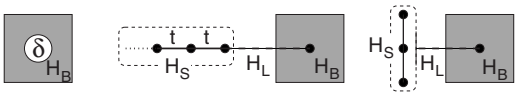

FIG. 1. Different system-bath geometries used for examples in this paper. On the left, a single site is embedded in a host [see Eq. (18)], e.g., an impurity in a lattice. In the middle, a chain is coupled to a bath [see Eq. (28)], allowing an electron to move along the chain and to hop to the bath and return. On the right, a single site with local bosonic degrees of freedom is coupled to a bath [see Eq. (35)]. An electron can excite bosons at the site, and hop to the bath while the bosons are left behind. The last two cases fit into the scheme of Eq. (6), where the coupling between system and bath is given by a Hamiltonian H_L.

The idea we promote here provides a different solution which is based on Chebyshev expansions of spectral functions of the bath. The Chebyshev expansion supplies the information necessary for an exact calculation of correlations function for the quantum system coupled to the bath, but avoids the introduction of redundant parameters that unnecessarily complicate the calculation. Thereby, the simplification of a noninteracting bath is exploited while the full coupled dynamics of the quantum system and the bath is retained. The realization of this idea amounts to the construction of an abstract vector space, which we call the Chebyshev space (CS). The combination of the CS with computational techniques based on Chebyshev expansions, in particular, KPM, will be referred to as the Chebyshev space method (CSM).

We demonstrate the CSM in this paper for a number of examples (see Fig. 1), including (i) the calculation of spectral functions and ground state energy for an impurity in a host in various dimensions, (ii) the description of the electron-polaron phase transition for a bosonic impurity, (iii) the self-consistent solution of the Holstein model within DMFT, and (iv) the time propagation of a wave packet on a chain with different boundary conditions.

We do not include examples for interacting fermions at finite density that involve renormalization of the bath due to the creation of particle-hole pairs like in the Kondo problem. The discussion would exceed a tolerable length of this paper and obscure the presentation of the other ideas. We return to this issue in the conclusion, and concentrate here on examples better suited for the introduction of the technical details of the CS construction.

The paper is organized as follows. In Sec. II, we remind the reader of Chebyshev expansions for spectral functions, and fix some notations used in the remainder. In Sec. III, we introduce the CS, and explain in Sec. IV the implementation of the CSM for the example of an impurity embedded in a host. In Sec. V, we derive an important property of the CS and discuss its practical relevance. Section VI describes how self-consistent calculations are performed in CSM, and Sec. VII demonstrates how the concurrent dynamics of a quantum system and a bath, when degrees of freedom evolve in parallel, is accounted for. This provides the basis for the study of the phase transition for a bosonic impurity in Sec. VIII, and to the self-consistent solution of the Holstein model within DMFT in Sec. VIII A. In Sec. IX, we address the time evolution of a wave packet on a long chain with different boundary conditions realized by CSM. We summarize in Sec. X and point out possible future advancements of CSM. In the Appendixes, we provide a short account of technical aspects of Chebyshev expansions and KPM, and the derivation of some mathematical results used in the text.

II. CHEBYSHEV EXPANSIONS AND THE KERNEL POLYNOMIAL

The recurrent theme of this paper is the expansion of a spectral function in a series of Chebyshev polynomials. To make the paper self-contained, we add an appendix on technical issues of Chebyshev expansions and KPM (Appendix A). For a more detailed exposition, we refer the reader to the recent review Ref. 5, and references cited therein.

The Chebyshev polynomials $T_n(x)$ are defined by the two-term recurrence,[10]

$$T_0(x) = 1, \quad T_1(x) = x,$$

$$T_{n+1}(x) = 2xT_n(x) - T_{n-1}(x), \tag{1}$$

which is equivalent to $T_n(x)=\cos(n \arccos x)$. The Chebyshev polynomials are mutually orthogonal on the interval $[-1,1]$ with respect to the scalar product given by the weighting function $(1-x^2)^{-1/2}$, obeying the relations

$$\int_{-1}^{1} \frac{T_m(x)T_n(x)}{\pi\sqrt{1-x^2}}dx = \begin{cases} 1, & n=m=0 \\ \frac{1}{2}\delta_{mn}, & n,m \neq 0. \end{cases} \tag{2}$$

Equation (2) implies that the Chebyshev polynomials form an orthogonal basis for functions defined on the interval $[-1,1]$. To expand a spectral function, defined as

$$A(\omega) = \langle\psi|\delta(\omega - H)|\psi\rangle = -\frac{1}{\pi}\lim_{\eta\to 0^+} \mathrm{Im}\langle\psi|[\omega + i\eta - H]^{-1}|\psi\rangle \tag{3}$$

to some Hamiltonian H and vector $|\psi\rangle$, in a series of Chebyshev polynomials it must, therefore, vanish outside $[-1,1]$. This can be achieved by rescaling the Hamiltonian H as $H=p\tilde{H}+q$, where p,q is chosen in such a way that all eigenvalues of $\tilde{H}$ lie in $[-1,1]$, or equivalently $\|\tilde{H}\|<1$. After a corresponding variable substitution $x=(\omega-q)/p$, the Chebyshev expansion for $A(x)$ reads

$$A(x) = \frac{1}{\pi\sqrt{1-x^2}}\left[\mu_0 + 2\sum_{n=1}^{\infty}\mu_n T_n(x)\right], \tag{4}$$

for $A(\omega)$ on the interval $[\omega_{\min},\omega_{\max}]$ with $\omega_{\min}=-p+q$, $\omega_{\max}=p+q$. Comparing this expansion to the definition (3), and using the orthogonality relation (2), we find that the coefficients in this series—the Chebyshev moments—are given by

$$\mu_n = \int_{-1}^{1} T_n(x)A(x)dx = \langle\psi|T_n(\tilde{H})|\psi\rangle. \tag{5}$$

We will assume in the following that any Hamiltonian is properly scaled to $[-1,1]$. The introduction of scaling factors is straightforward most times. Whenever important, we will explicitly discuss the consequences of scaling.

The calculation of the vectors $T_n(\tilde{H})|\psi\rangle$ in Eq. (5) can be accomplished by means of the two-term recurrence (1). Starting with the vector $|\psi\rangle$, one iteratively obtains the $(n+1)$th vector from the nth and $(n-1)$th vector. The calculation of the moments, therefore, requires (i) to apply H to a vector, i.e., to perform matrix-vector multiplication if H is explicitly given as a matrix, and (ii) to evaluate a scalar product of two vectors.

In any practical application only a finite number N of moments can be calculated, and $A(\omega)$ has to be reconstructed from a truncated series, taking the first N terms in Eq. (4). The reconstruction of $A(\omega)$ from such a finite series is the issue of KPM (see Appendix A). High resolution of $A(\omega)$ is already obtained with a fairly small number of moments, thus allowing for accurate calculations with moderate demands on computational time or memory. The resolution of KPM scales linearly with N. It is usually much better than for the Lanczos (recursion) method,[11–13] and can be unrestrictedly increased without problems.[5]

III. GENERAL SCHEME

A coupled quantum system and bath is generally described by a Hamiltonian of the form[6,14]

$$H = H_S + H_L + H_B. \tag{6}$$

H_S and H_B denote the Hamiltonian for the quantum system and the bath, respectively, and H_L describes the coupling between system and bath. Without coupling, for $H_L=0$, the degrees of freedom of the quantum system and the bath evolve independently, i.e., H_S and H_B commute. We restrict ourselves in this paper to situations with a single spinless fermion. This allows to introduce the CS without a discussion of complications inherent to many-fermion physics. The CSM can be extended to finite fermion density, or the inclusion of spin degrees of freedom, with the same implementation of a CS as given in this paper. We return to that issue in Sec. X.

Since the bath consists of noninteracting fermions, H_B is a bilinear Hamiltonian

$$H_B = \sum_{\alpha\beta} (H_B)_{\alpha\beta} f_\alpha^\dagger f_\beta, \tag{7}$$

where $f_\alpha^{(\dagger)}$ are fermionic operators for the bath degrees of freedom. The indices α,β can denote, e.g., an arbitrary set of orbitals, sites of a lattice, or, if $(H_B)_{\alpha\beta}$ is diagonal, the eigenstates of H_B. A change of indices corresponds to a unitary transformation of the matrix $(H_B)_{\alpha\beta}$. The system Hamiltonian H_S can be of arbitrary form, involving any type of interaction. We do not specify H_S now, and discuss examples for various different H_S later.

More can be said about the coupling term H_L. In general, the bath is in contact to one (or a few) site(s) of the quantum system, say, site 0 with fermionic operator $c_0^{(\dagger)}$. Fermions hop from this site to the bath, and back. The appropriate choice for H_L is

$$H_L = \sum_\alpha t_\alpha (c_0^\dagger f_\alpha + f_\alpha^\dagger c_0) \quad (t_\alpha \in \mathbb{R}), \tag{8}$$

or a sum of terms of this form. It is convenient to introduce a fermionic operator $d^{(\dagger)}$ by

$$d^\dagger = \sum_\alpha a_\alpha f_\alpha^\dagger, \quad a_\alpha = t_\alpha \Big/ \left(\sum_\alpha t_\alpha^2\right)^{1/2}. \tag{9}$$

As $\Sigma_\alpha a_\alpha^2 = 1$, the fermionic anticommutator relation $\{d,d^\dagger\} = 1$ is fulfilled. With the introduction of $d^{(\dagger)}$, H_L acquires the form of a hopping term between two sites,

$$H_L = V(c_0^\dagger d + d^\dagger c_0), \quad V = \left(\sum_\alpha t_\alpha^2\right)^{1/2}. \tag{10}$$

Depending on the meaning of indices in Eq. (7), d can denote a concrete orbital or a site in a lattice, or just an abstract linear combination of f operators. If we think of a mesoscopic system contacted to a lead, then $c_0^{(\dagger)}$ and $d^{(\dagger)}$ denote operators for the contact point in the system and lead, respectively.

We define the bath spectral function $A_B(\omega)$ as the spectral function of the d orbital,

$$A_B(\omega) = \langle \text{vac}|d\delta(\omega - H_B)d^\dagger|\text{vac}\rangle, \tag{11}$$

where $|\text{vac}\rangle$ is the bath vacuum, i.e., $d|\text{vac}\rangle = 0$. Remember that we study situations with a single fermion. For finite fermion density, we had to consider both the particle and hole part of the spectral function, and to account for Pauli blocking.

After the transformation (9), the bath occurs in the calculation of correlation functions for the quantum system only through the spectral function $A_B(\omega)$ and the coupling strength V. The precise coefficients in Eqs. (7) and (8) do not occur. In this sense, all Hamiltonians (6) with the same $A_B(\omega)$, V, but potentially different H_B, H_L, are equivalent. Often, the problem under study is defined in this way, by specifying $A_B(\omega)$ and V, without an explicit representation of H_B or H_L as in Eqs. (7) and (8) at hand.

Given such a problem, how can it be accessed within numerically exact techniques such as Lanczos or KPM? Since these techniques need the Hamiltonian H explicitly given, it seems inevitable to use an explicit representation of H_B in the form (7). One possible way to obtain such a representation is to discretize $A_B(\omega)$ by a finite number of δ peaks, as

$$A_B(\omega) \approx \sum_\alpha w_\alpha \delta(\omega - \epsilon_\alpha). \tag{12}$$

This approximation translates to $H_B = \Sigma_\alpha \epsilon_\alpha f_\alpha^\dagger f_\alpha$, and $d^\dagger = \Sigma_\alpha w_\alpha^{1/2} f_\alpha^\dagger$. A calculation then relies on our ability to construct a good approximation (12). This poses certain questions: How to choose the positions ϵ_α of peaks, how to choose their weights w_α, and how many of them are needed

to approximate $A_B(\omega)$ sufficiently well? When is an approximation to $A_B(\omega)$ sufficiently good, and what is the precise meaning of "≈" in Eq. (12)? Is there an optimal way to choose ϵ_α, w_α for a given number of peaks? While the result of a calculation for the quantum system does not depend on the precise form of H_B, it does depend on the approximation for H_B or $A_B(\omega)$. How can we control this dependence? There is no definite answer to these questions, and the need to discretize $A_B(\omega)$ is quite unsatisfactory. Our proposition, the use of the CS in the CSM, avoids the discretization of $A_B(\omega)$. It works without a representation of H_B in the form (7), but addresses H_B only via the spectral function $A_B(\omega)$.

The central ingredient of CS(M) is a representation of H_B related to the Chebyshev expansion of $A_B(\omega)$. To obtain this representation, define the Chebyshev vectors

$$|n\rangle = T_n(H_B)d^\dagger|\text{vac}\rangle \tag{13}$$

for $n \geqslant 0$. These vectors are neither normalized nor orthogonal. We need only the scalar products

$$\langle 0|n\rangle = \langle \text{vac}|dT_n(H_B)d^\dagger|\text{vac}\rangle = \mu_n^B, \tag{14}$$

where μ_n^B is the nth Chebyshev moment of the bath spectral function $A_B(\omega)$, according to the expansion (4). The Chebyshev vectors span a Hilbert space $\mathcal{H}_c$, the CS. By definition, $\mathcal{H}_c$ is a subspace of the Fock space for the bath operators $f^{(\dagger)}$, but we refer to the Chebyshev vectors only as abstract vectors, whose possible representation in terms of the $f^{(\dagger)}$ is irrelevant.

From the recurrence relation (1), it follows that the operation of H_B on $\mathcal{H}_c$ is given by

$$H_B|n\rangle = \begin{cases} |1\rangle, & n = 0 \\ (1/2)(|n-1\rangle + |n+1\rangle), & n \neq 0. \end{cases} \tag{15}$$

Since $|n\rangle$ is a one-fermion state, $d|n\rangle$ is proportional to $|\text{vac}\rangle$. Together with the definition of μ_n^B this yields

$$d|n\rangle = dT_n(H_B)d^\dagger|\text{vac}\rangle = |\text{vac}\rangle\langle\text{vac}|dT_n(H_B)d^\dagger|\text{vac}\rangle = \mu_n^B|\text{vac}\rangle \tag{16}$$

and

$$\begin{aligned} d^\dagger d|n\rangle &= d^\dagger dT_n(H_B)d^\dagger|\text{vac}\rangle \\ &= d^\dagger|\text{vac}\rangle\langle\text{vac}|dT_n(H_B)d^\dagger|\text{vac}\rangle = \mu_n^B|0\rangle. \end{aligned} \tag{17}$$

The reader should note that in these equations the only parameters are the Chebyshev moments μ_n^B of the spectral function $A_B(\omega)$.

Equations (14)–(17) constitute the basis of our CS approach. What we have achieved is that H_B is put into a form that makes no reference to a representation such as (7). Still, H_B is given as a Hamiltonian acting on a Hilbert space. This is a very useful form for H_B, which can be used within numerically exact techniques like Lanczos or KPM *and* avoids discretization of $A_B(\omega)$.

IV. FERMIONIC SITE EMBEDDED IN A HOST

We illustrate the use of the CS(M) with the example

$$H = -\Delta d^\dagger d + H_B \tag{18}$$

of an unperturbed system H_B with a perturbation $-\Delta d^\dagger d$. This is the Hamiltonian of a single site in a sea of noninteracting fermions, like an impurity embedded in a host or lattice. Note that this example is not of the form (6), as it deals with a site embedded in the bath, while in Eq. (6) and later examples fermions leave the bath by hopping to the quantum system.

Our goal is to calculate the spectral function

$$A(\omega) = \langle \text{vac}|d\delta(\omega - H)d^\dagger|\text{vac}\rangle \tag{19}$$

to given $A_B(\omega)$ and Δ within CSM, i.e., using KPM with the Eqs. (14)–(17) for the CS. We can compare the results to the exact result

$$G(z) = [G_B(z)^{-1} + \Delta]^{-1} \tag{20}$$

for the corresponding Green functions

$$G_{(B)}(z) = \langle \text{vac}|d[z - H_{(B)}]^{-1}d^\dagger|\text{vac}\rangle. \tag{21}$$

To obtain the Chebyshev moments μ_n of $A(\omega)$, we have to recursively calculate the vectors $T_n(H)d^\dagger|\text{vac}\rangle$ according to Eq. (1). The calculation proceeds in the space $\mathcal{H}_c$, and each vector is given as a linear combination of Chebyshev vectors $|n\rangle$. With H_B according to Eq. (15) and $\Delta d^\dagger d$ according to Eq. (17), H is represented by the matrix

$$(H)_{mn} = \frac{1}{2}\begin{pmatrix} -2\Delta\mu_0^B & 1-2\Delta\mu_1^B & -2\Delta\mu_2^B & -2\Delta\mu_3^B & \cdots \\ 2 & 0 & 1 & 0 & \cdots \\ & 1 & 0 & 1 & \\ & & 1 & 0 & \\ & & \vdots & & \ddots \end{pmatrix}, \tag{22}$$

with $H|n\rangle = \Sigma_m (H)_{mn}|m\rangle$. Note that $(H)_{mn} \neq \langle m|H|n\rangle$, because the Chebyshev vectors are not orthogonal. Especially, $(H)_{mn}$ is not symmetric. Nevertheless, H is Hermitian by definition (an explicit calculation is given in Appendix C).

Starting with the vector $|0\rangle = d^\dagger|\text{vac}\rangle$, in any step of the Chebyshev iteration we apply H according to Eq. (22) to obtain the vector $T_n(H)|0\rangle$ from previous vectors $T_{n-1}(H)|0\rangle$, $T_{n-2}(H)|0\rangle$. The moment μ_n is finally obtained from the scalar product $\langle 0|T_n(H)|0\rangle$ according to Eq. (14). During the iteration, the index of any vector $|n\rangle$ is increased at most by 1 in Eq. (22), and the vector $T_n(H)|0\rangle$ is a linear combination of Chebyshev vectors $|m\rangle$, with $m \leqslant n$. The nth Chebyshev moment μ_n of $A(\omega)$ is therefore obtained from the first n Chebyshev moments $\mu_0^B, \ldots, \mu_n^B$ of $A_B(\omega)$. We have thus devised a computational scheme to map n moments of a given spectral function $A_B(\omega)$ to one part H_B of H to n moments of a spectral function $A(\omega)$ to the full Hamiltonian H *without* resorting to an explicit representation (7) of H_B in an orbital basis $f_\alpha^\dagger$. This is the essence of CSM.

Note that only spectral functions $A_B(\omega)$, $A(\omega)$ occur in the calculation. The "missing" real part of the corresponding Green function, which is needed in Eq. (20), is implicitly accounted for by causality relations preserved in the calcula-

tion. As shown in Ref. 5, we can obtain the Green function $G(\omega)$ from moments μ_n of the spectral function $A(\omega)$ without invoking Kramers-Kronig relations.

A. Scaling of H and H_B

We have so far omitted the scaling of H and H_B to the interval $[-1,1]$. To determine the scaling of H_B, we must choose a scaling interval I_B that contains the domain of nonzero values of $A_B(\omega)$, i.e., $A_B(\omega)=0$ for $\omega \notin I_B$ (see Sec II). For $I_B=[\omega^B_{\min},\omega^B_{\max}]$, the scaling factors

$$r=(\omega^B_{\max}-\omega^B_{\min})/2, \quad s=(\omega^B_{\min}+\omega^B_{\max})/2 \tag{23}$$

give the scaling $H_B=r\tilde{H}_B+s$ of H_B. The smaller I_B, the higher is the resolution of $A_B(\omega)$ for a given number of moments. Similarly, we choose a scaling interval I with $A(\omega)=0$ for $\omega \notin I$. With scaling factors p, q determined from I as before, we find for the scaling of H

$$\tilde{H}=\frac{1}{p}(H-q)=\frac{-\Delta}{p}d^\dagger d+\frac{r}{p}\tilde{H}_B+\frac{s-q}{p}. \tag{24}$$

It is straightforward to introduce the scaling factors into Eqs. (15) and (16) and the matrix form (22).

Since we do not know $A(\omega)$ in advance, we have to rely on estimates for I. For Eq. (18), the term $-\Delta d^\dagger d$ has eigenvalues 0 and $-\Delta$. It follows that any I with $I \supset I_B \cup (I_B-\Delta)$ is a possible choice. Similar estimates can be obtained in other situations. Alternatively, we can determine the minimal and maximal eigenvalues of H by the Lanczos algorithm (see Sec. VIII). Note that precise knowledge of the minimal or maximal eigenvalue of H is not necessary, but any bound works. It often suffices to obtain an estimate from operator norms. A factor of the order of 2 in the scaling is tolerable for most practical purposes. The resolution of CSM—or KPM—still compares quite favorably to the resolution of other techniques. The possible loss of resolution for a too large I can be compensated for by increasing the number of moments in the calculation. We show in Sec. V that we can even increase the resolution for $A(\omega)$ without increasing the number of moments for $A_B(\omega)$.

The reader should be reminded that the need to consider scaling is the price one has to pay for the high resolution of the Chebyshev technique—this is certainly no drawback of the method. Interestingly, there are situations where the divergence of moments for wrong scaling can be used to our advantage: We will exploit it below to determine the ground state energy of H.

Now consider the case $\Delta=0$ in Eq. (18). We know that then $A(\omega)=A_B(\omega)$. With scaling intervals $I \supset I_B$, the moments μ_n, μ^B_n of these two identical functions are different since $I \neq I_B$. We can use CSM to calculate the μ_n, reproducing $A_B(\omega)$ on the larger interval I (see next section). Now assume that we choose I_B much larger than necessary. In principle, a possible scaling interval I for H might then be smaller than I_B, i.e., $I \subset I_B$. Will CSM then reproduce the spectral function $A_B(\omega)$, respectively, its moments, on the smaller interval I?

The answer is no: The interval I must always be larger than I_B, i.e., $I \supset I_B$. Then, and only then, the Chebyshev iteration for $\Delta=0$, and $H=H_B$, is stable in the space $\mathcal{H}_c$. This can be understood from the fact that H_B acts within $\mathcal{H}_c$ like an operator with unity norm: The column sums of the matrix (22) for $\Delta=0$ are unity, and the first column has a single unity entry. Note that this is a statement about the norm of H_B as a matrix, and not with respect to the scalar product of Chebyshev vectors. If now $I \subset I_B$, then $r/p>1$, and $(r/p)\|\tilde{H}\|>1$ in Eq. (24). Then, the coefficients in front of the Chebyshev vectors $|n\rangle$ diverge during the iteration, while the moments μ^B_n decay with the same rate. Each moment μ_n is a sum of products of coefficients and moments μ^B_n. Within exact arithmetics, the correct moments μ_n would be reproduced. In finite precision arithmetics, however, numerical round-off errors entirely ruin the output. On the contrary, for $I \supset I_B$, the recursion is perfectly stable, up to any number of moments. This is an important point to be aware of.

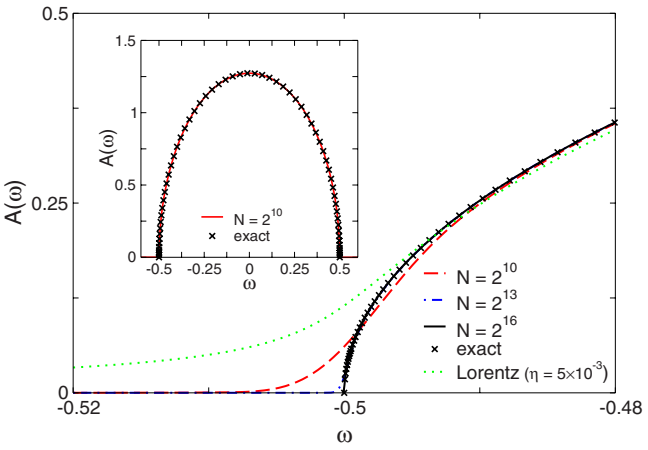

FIG. 2. (Color online) Spectral function $A(\omega)$ for semicircular $A_B(\omega)$ according to Eq. (25), with $W=1$ and $\Delta=0$. The scaling intervals are $I_B=[-0.6W,0.6W]$ and $I=[-1.2W,1.2W]$, i.e., $r/p=0.5$ in Eq. (24). The figure displays the region around the lower band edge $\omega=-W/2$, with curves for $N=2^{10},2^{13},2^{16}$ Chebyshev moments, the exact result, and a curve with Lorentzian broadening $\eta/(\omega^2+\eta^2)$ to $\eta=5\times10^{-3}$. The latter curve illustrates the typical quality of results from the Lanczos recursion method. With $N=2^{10}$ Chebyshev moments, the exact curve is much better reproduced than with Lorentzian broadening. The inset shows the full curve, whose deviation from the exact result is below linewidth on this scale. The curve for $N=2^{16}$ lies on top of the exact result even in magnification of the band edge, and demonstrates that CSM can achieve arbitrary precision.

B. Numerical results

We now show results from CSM for the model defined in Eq. (18). We start with a semicircular spectral function

$$A_B(\omega)=\frac{8}{\pi W^2}\sqrt{W^2/4-\omega^2}, \quad |\omega| \leq W/2, \tag{25}$$

realized, e.g., as the density of states in a Bethe lattice. W is the bandwidth. The first test of CSM is the calculation of $A(\omega)$ for $\Delta=0$ in Fig. 2. Then, $A(\omega)=A_B(\omega)$, and the numerics has to reproduce Eq. (25) on an interval I different from

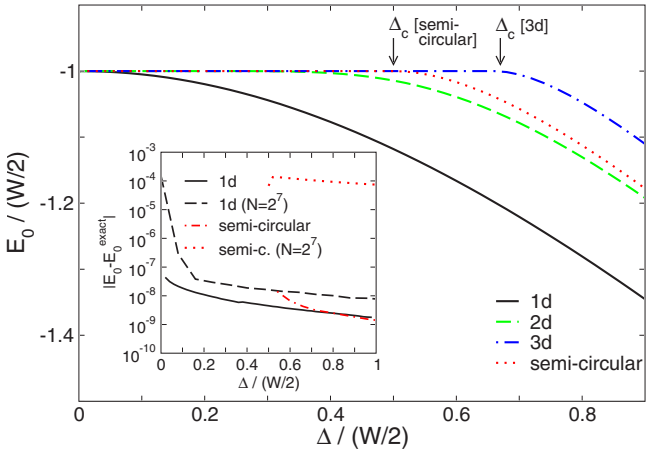

FIG. 3. (Color online) Ground state energy $E_0(\Delta)$ for an impurity in 1D, 2D, and 3D lattices, and with a semicircular density of states. $E_0(\Delta)$ is calculated with the method described in text, for $N=2^{10}$ Chebyshev moments. The arrows indicate the critical Δ_c, with $\Delta_c(\text{semicircular})=W/4$ and $\Delta_c[3d]\approx 0.330\times W$. The inset displays the error to the exact result for 1D and semicircular density of states, where a simple exact result for $E_0(\Delta)$ is available. Already for $N=2^7$ moments, we obtain results with an error below 10^{-4}. For 1D, the error decreases rapidly for larger Δ, since the ground state is then strongly localized at the impurity, and the band edge singularity of the density of states less important.

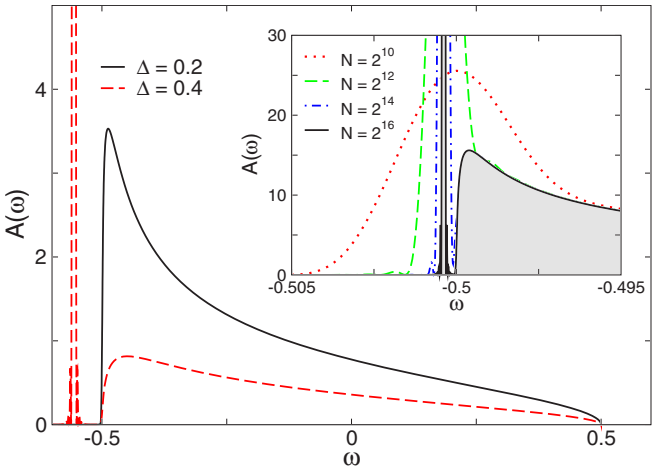

FIG. 4. (Color online) Spectral function $A(\omega)$ for semicircular $A_B(\omega)$ (Eq. (25)), with $W=1$ and finite Δ. The scaling intervals are $I_B=[-(0.5+\epsilon)W,(0.5+\epsilon)W]$ and $I=[-(0.5+\epsilon)W-\Delta,(0.5+\epsilon)W]$, with a small offset $\epsilon=10^{-4}$. For $\Delta>\Delta_c=W/4$, $A(\omega)$ has a pole outside the band of continuum states (cf. Fig. 3). The deviation of the curves with $N=2^{10}$ to the exact result is below linewidth, except for the pole in the curve for $\Delta=0.4$, which attains a finite width. The inset displays four curves for $\Delta=0.26$ and different N. For this Δ, $A(\omega)$ has a pole at $E_0(\Delta)\approx -W/2-3.846\times 10^{-4}$. Although the pole is separated from the band edge $-W/2$ by less than 10^{-3} times the bandwidth W, it can be resolved within CSM provided N is large enough. It is hardly possible to achieve a similar increase in resolution with e.g. the Lanczos Recursion Method.

I_B. In particular, the moments μ_n and μ_n^B are not identical.

We expect strongest deviations from the numerical result to Eq. (25) close to the band edges, where the spectral function behaves like a square root. For $N=2^{10}$ moments, the absolute deviation $|A^n(\omega)-A^e(\omega)|$ between numerical $[A^n(\omega)]$ and exact $[A^e(\omega)]$ spectral function is smaller than 6×10^{-2} at the band edge, and smaller than 5×10^{-5} over the remaining 90% of the band. The cumulative deviation $\int|A^n(\omega)-A^e(\omega)|d\omega$ is below 10^{-4}. Notably, the resolution is much higher than for other methods, e.g., using the Lanczos recursion method with Lorentzian broadening of the spectral function. Note also that the twofold Chebyshev recursion—once for the moments of $A_B(\omega)$, once for $A(\omega)$—is perfectly stable for any number of moments. The calculation of many thousand of Chebyshev moments is no problem, allowing for unprecedented resolution.

To further test the accuracy of our approach, we calculate the ground state energy $E_0(\Delta)$ of an impurity in an infinite chain [one-dimensional (1D)], square [two-dimensional (2D)], cubic [three-dimensional (3D)] tight-binding lattice, and for the semicircular density of states in Eq. (25) (see Fig. 3). For sufficiently large Δ, a bound state at the impurity exists, with energy outside the band of continuum states, i.e. $E_0(\Delta)<-W/2$. In 1D and 2D, a bound state exists for any $\Delta>0$, while in 3D and for the semicircular density of states a bound state exists above a critical value Δ_c. In Fig. 4, we show the impurity spectral function for $\Delta\neq 0$. $A(\omega)$ has a δ peak at $\omega=E_0$ if $\Delta>\Delta_c$. Even if the peak is very close to the band edge, it can be resolved within CSM by increasing the number of moments N.

To find $E_0(\Delta)$ within CSM, we exploit the possible divergence of moments in the Chebyshev recursion. We initially choose a scaling interval $I=[\omega_{\min},\omega_{\max}]$ for H so large that moments do not diverge. Then we vary $\omega_{\min}$. If the moments diverge, $E_0<\omega_{\min}$, otherwise $E_0\geqslant\omega_{\min}$. Using, e.g., a bisection algorithm on $\omega_{\min}$, we can calculate E_0 to high precision. The computational effort for Fig. 3 is independent of the lattice dimension, as only a fixed number of moments enter the calculation. The most demanding case here is indeed 1D, as the spectral function diverges at the band edge. Despite this particular complication, the results are extremely accurate already for $N=2^{10}$ moments.

For our example, E_0 is the ground state energy of a single particle, i.e., the smallest energy with $A(E_0)\neq 0$. The weight $A(E_0)$ can be arbitrarily small. From Eq. (20), we see that $A(\omega)\neq 0$ whenever $A_B(\omega)\neq 0$. Within the numerics, the domain of nonzero values of $A_B(\omega)$ is fixed by the scaling interval $I_B=[\omega_{\min}^B,\omega_{\max}^B]$. We also know from the previous section, that moments diverge for $\omega_{\min}>\omega_{\min}^B$. As a consequence, the calculation results in $E_0\leqslant\omega_{\min}^B$. Therefore, $\omega_{\min}^B$ must be chosen at the lower band edge of $A_B(\omega)$, i.e., $\omega_{\min}^B=-W/2$ in all examples. As long as $|E_0|>|\omega_{\min}^B|$, especially for $\Delta>\Delta_c$, no problem occurs. Note that the situation is different at finite fermion density, where the ground state energy is determined by filling states up to a certain density n, with $n=\int_{-\infty}^{E_0}A(\omega)d\omega$. Negligible weight in $A(\omega)$ does not change E_0 then, and the calculated E_0 does not depend that strongly on I_B.

From the examples shown here, we conclude that CSM provides highest accuracy. The computational effort to obtain the results shown is small—a calculation for $N=2^{10}$ takes

less than a second—which leaves plenty of room for applications to less simple problems. In the next section, we discuss how the computational effort can be further reduced, by adjusting the resolution of the two Chebyshev expansions for $A(\omega)$ and $A_B(\omega)$.

V. PROPERTIES OF THE TRUNCATED CHEBYSHEV REPRESENTATION OF H_B

In the examples of the previous section, we calculate N moments of $A(\omega)$ from the same number of moments of $A_B(\omega)$. Calculations can also be performed for a different number of moments of $A_B(\omega)$, say, M. For $M \geqslant N$, the moments of $A(\omega)$ do not change and the calculation is exact, as we noted above. For $M<N$, however, the calculation is approximate and its result depends on M.

The computational effort for given M,N scales as $O(MN)$ for time, and $O(M)$ for memory: Calculating more moments of $A(\omega)$ requires only more time, while using more moments of $A_B(\omega)$ requires more time and memory. It is, therefore, natural to ask whether we can obtain N moments of $A(\omega)$ from fewer moments of $A_B(\omega)$, especially if we remember that both are calculated with different scalings for H and H_B. We know that the resolution of a Chebyshev expansion increases linearly with the number of moments, as can be deduced, e.g., from the width (standard deviation) $\sigma=\pi/N$ of the Jackson kernel, see Appendix A. If we demand that the resolution for $A(\omega)$ and $A_B(\omega)$ is the same, we obtain the condition $M/N \gtrsim r/p$, with the scaling $H=p\tilde{H}+q$, $H_B=r\tilde{H}_B+s$ as in Eq. (24). As we discussed there, the factor r/p is always smaller than unity. For the example of the Holstein model in Sec. VIII A, it is easily of the order 10^{-1}.

In Fig. 5, we show $A(\omega)$ for different ratios M/N. As long as the condition $M/N \gtrsim r/p$ is fulfilled, we produce an absolutely accurate $A(\omega)$ from $M<N$ moments of $A_B(\omega)$, while the computational effort is considerably reduced. In the worst case, for $M/N \ll r/p$, discrete energy levels in the truncated bath Hamiltonian H_B^M are resolved. Even $N \gg M$ does not lead to erroneous results as a negative spectral function. In particular, the CSM is perfectly stable for arbitrary N and M.

Using $M<N$ moments of $A_B(\omega)$ in the calculation is equivalent to working with a truncated bath Hamiltonian H_B^M on the M-dimensional subspace $\mathcal{H}_c^M$ of $\mathcal{H}_c$ that is spanned by vectors $|0\rangle,\ldots,|M-1\rangle$. The matrix of H_B^M, with $H_B^M|n\rangle = \Sigma_m (H_B^M)_{mn}|m\rangle$, is according to Eq. (15) the tridiagonal $M \times M$ matrix

$$(H_B^M)_{mn} = \frac{1}{2}\begin{pmatrix} 0 & 1 & & & & & \\ 2 & 0 & 1 & & & & \\ & 1 & 0 & 1 & & & \\ & & 1 & 0 & \ddots & & \\ & & & \ddots & 0 & 1 & \\ & & & & 1 & 0 & 1 \\ & & & & & 1 & 0 \end{pmatrix}. \tag{26}$$

We show in Appendix B, that the characteristic polynomial of $(H_B^M)_{mn}$ is

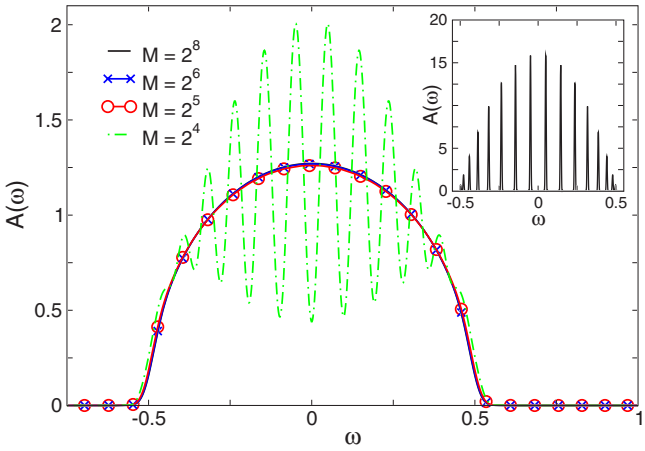

FIG. 5. (Color online) Similar to Fig. 2, this figure shows the spectral function $A(\omega)$ for semicircular $A_B(\omega)$ according to Eq. (25), with $W=1$ and $\Delta=0$. The scaling intervals are $I_B=[-(0.5+\epsilon)W,(0.5+\epsilon)W]$ with $\epsilon=10^{-4}$ and $I=[-2W,2W]$, i.e., $r/p=1/4$ in Eq. (24). The calculation is performed for $N=2^8$ Chebyshev moments of $A(\omega)$ and M moments of $A_B(\omega)$. As long as $M/N \gtrsim r/p$, i.e., here $M \gtrsim 2^6$, the result cannot be distinguished from the (numerically exact) curve for $M=N$. For $M=2^5$, deviations occur at the band edges, and for $M=2^4$ single spurious peaks are resolved. The inset displays a calculation for $N=2^{11}$ and $M=2^4$. Even for this strong mismatch, a perfectly positive spectral function is obtained, resolving δ peaks at $\omega_j=rx_j+s$ corresponding to the roots x_j of $T_M(x)$ (see text).

$$\det[x-(H_B^M)_{mn}] = 2^{-(M-1)}T_M(x). \tag{27}$$

The Mth Chebyshev polynomial $T_M(x)=\cos(M \arccos x)$ has M distinct real roots $x_j=\cos\frac{\pi(j-1/2)}{M}$ for $j=1,\ldots,M$. It follows that $(H_B^M)_{mn}$ has M distinct real eigenvalues, hence H_B^M is a diagonalizable $M \times M$ matrix with real eigenvalues x_j. The position of the discrete energy levels resolved for $N \gg M$ in Fig. 5 is determined by the x_j. We discuss in Appendix D how the weight of the corresponding peaks can be obtained from the moments μ_m^B.

VI. LINEAR CHAIN COUPLED TO A BATH

A different example is provided by an electron hopping along a finite chain of length L that is connected to a bath at its "right" end (site L). The Hamiltonian

$$H = -t\sum_{i=1}^{L-1}(c_{i+1}^\dagger c_i + c_i^\dagger c_{i+1}) + H_L + H_B \tag{28}$$

has the form of Eq. (6). Here, $c_i^\dagger$ creates an electron at lattice site i, and the coupling between chain and bath is $H_L=-t(d^\dagger c_L + c_L^\dagger d)$, as in Eq. (10), with $V=-t$. That the bath couples to the d orbital implies that $[c_i^{(\dagger)},H_B]=0$, but $[d^{(\dagger)},H_B] \neq 0$.

In difference to the example in Sec. IV [see Eq. (18)], the particle hops to and from the bath, hence the Hilbert space $\mathcal{H}=\mathcal{H}_S \oplus \mathcal{H}_c$ of the problem is the direct sum of the Hilbert space $\mathcal{H}_S$ of the chain and the CS $\mathcal{H}_c$. A basis of $\mathcal{H}_S$ consists of vectors $|\psi_i\rangle=c_i^\dagger|\text{vac}\rangle$, for the electron at site i. The vectors

$|\psi_i\rangle$ are orthogonal to the Chebyshev vectors $|n\rangle$. The operation of H is summarized in

$$H|\psi_1\rangle = -t|\psi_2\rangle,$$

$$H|\psi_i\rangle = -t|\psi_{i+1}\rangle - t|\psi_{i-1}\rangle \quad \text{for } i = 2, \ldots, L-1,$$

$$H|\psi_L\rangle = -t|0\rangle - t|\psi_{L-1}\rangle,$$

$$H|n\rangle = -t\mu_n^B|\psi_L\rangle + H_B|n\rangle, \tag{29}$$

with the missing equations supplied by Eq. (15).

The calculation of the spectral function $A_{11}(\omega) = \langle \text{vac}|c_1 \delta(\omega - H) c_1^\dagger|\text{vac}\rangle$—the spectral function to the "left" end of the chain in Fig. 1—to given bath spectral function $A_B(\omega)$ proceeds along the lines established in Sec. IV. In contrast to the example (18), where Eq. (14) was used, scalar products with the starting vector $c_1^\dagger|\text{vac}\rangle$ of the Chebyshev iteration do not involve the μ_n^B.

To make the present example self-consistent, we demand that $A_{11}(\omega) = A_B(\omega)$. The self-consistent solution $A_{11}(\omega)$ is the spectral function of a half-infinite chain at its open end, i.e., the semicircular spectral function from Eq. (25) with $W=4t$. To obtain the self-consistent $A_{11}(\omega)$, we start with an initial guess for $A_B(\omega)$, e.g., setting $\mu_n^B = 0$ corresponding to $A_B(\omega) = 0$, and calculate the moments μ_n of $A_{11}(\omega)$. Note that the choice $\mu_n^B = 0$ does not correspond to a spectral function, as the sum rule $\int A_B(\omega) d\omega = \mu_0^B = 1$ is violated. This does not matter for the calculation, and we could obtain the same effect by setting $V=0$. We start a new calculation taking the μ_n just calculated as new bath moments μ_n^B, and reiterate this calculation until the moments μ_n, or equivalently $A_{11}(\omega)$, are converged (see Fig. 6).

We found in Sec. IV that we must choose the scaling interval I for $A_{11}(\omega)$ larger than I_B for $A_B(\omega)$. If we start a new iteration with the previously calculated moments μ_n replacing μ_n^B, we must also replace the interval I_B by I, and consequently allow for growing scaling intervals—and corresponding loss of resolution—during the iterations. As an alternative, we keep the interval I_B fixed and rescale $A_{11}(\omega)$ from I to I_B in our implementation. We first construct $A_{11}(\omega)$ on the interval I from the μ_n, then rescale it in ω space to the interval I_B with a linear transformation $\omega \mapsto (r/p)(\omega - q) + s$ [see Eq. (24)], and finally feed the moments of this rescaled spectral function as new μ_n^B back into the calculation. In the rescaling, we can check whether we throw away significant weight of $A_{11}(\omega)$ which signals a too small I_B. For some examples where we do not know the relevant interval I_B in advance, e.g., for the Holstein polaron (Sec. VIII A), we let the program determine a suitable I_B that contains all but negligible weight of $A_{11}(\omega)$. Typically, the interval changes during the first few iterations and then stabilizes with convergence of $A_{11}(\omega)$. The rescaling transformation needs two Fourier transforms (preferentially fast Fourier transform) for the calculation of the spectral function from the moments and vice versa, and one interpolation for the linear scaling. We use spline interpolation, but for not too few moments everything also works without interpolation.

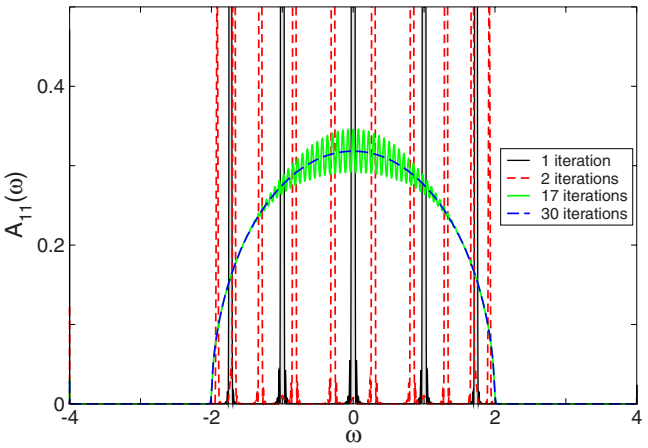

FIG. 6. (Color online) Spectral function $A_{11}(\omega)$ for a chain with $L=5$ sites, calculated for $N=N_B=2^{10}$ moments. In the first iteration, $A_{11}(\omega)$ consists of L peaks. The number of peaks is increased by L per iteration (see curve for 2 iterations). Peaks merge if their distance is smaller than the resolution (see curve for 17 iterations), until $A_{11}(\omega)$ is converged to the self-consistent semicircular solution after a sufficient number of iterations (here about 30 iterations). The scaling intervals are $I_B = [-(W/2+\epsilon), (W/2+\epsilon)]$, with $\epsilon = 10^{-4}$, and $I = [-W, W]$, with $W=4t$. Note that the number of iterations until convergence depends on the number of moments, i.e., the resolution. For $N=2^7$ moments, convergence is obtained after 6 iterations.

The reader should note that the rescaling transformation—which shrinks the ω interval of the Chebyshev expansion—is a linear transformation of moments $\{\mu_n\} \mapsto \{\mu_m^B\}$. A calculated μ_m^B depends on every μ_n. In contrast, the CSM of Sec. IV implements for $\Delta = 0$ in Eq. (18) a transformation $\{\mu_m^B\} \mapsto \{\mu_n\}$, that blows up the ω interval (see Fig. 2). An inspection of Eqs. (14) and (15) shows that this transformation is also linear. For $\Delta \neq 0$, it ceases to be linear as the μ_n^B also occur in H itself [see Eq. (22)], by virtue of Eq. (17). The transformation has the property that each calculated μ_n depends only on μ_m^B with $m \leqslant n$. We now understand a second reason why the Chebyshev iteration has to be unstable for $I_B \not\subset I$. If the Chebyshev iteration could be used to shrink the ω interval—that is for $I \subset I_B$—every calculated moment (μ_n) had to depend on every moment supplied to the calculation (μ_n^B), in contradiction to the properties of the recursion.

We discussed in Sec. V how to calculate with CSM N moments μ_n from M moments μ_m^B for $M < N$, depending on the scaling intervals I and I_B. Do we waste part of the numerical results if again only $M < N$ moments μ_m^B are calculated in the rescaling transformation? Obviously not: For a smaller interval, less moments are needed to obtain the same resolution. In both directions, via CSM or the rescaling transformation, the number of moments should be related by the estimate $M/N \sim r/p$.

VII. CONCURRENT DYNAMICS

The general Hamiltonian, Eq. (6), operates on a product space $\mathcal{H} = \mathcal{H}_S \otimes \mathcal{H}_B$. H_S (H_B) operates on $\mathcal{H}_S$ $(\mathcal{H}_B)$, and H_L

links the two spaces. In CSM, $\mathcal{H}_B=\mathcal{H}_c$. We can generally write the Hilbert space of H in such a way, with $\mathcal{H}_S$ and $\mathcal{H}_B$ as Fock spaces, but additional constraints may single out a subspace. In the example of the linear chain with the restriction to a single electron, $\mathcal{H}$ is the direct sum of $\mathcal{H}_S$ and $\mathcal{H}_c$.

Assume that system and bath do not couple, i.e., $H_L=0$ and $H=H_S+H_B$. As H_S and H_B commute, the spectral function $A(\omega)=\langle\psi|\delta(\omega-H)|\psi\rangle$ to a product state $|\psi\rangle=|\psi_S\rangle\otimes|\psi_B\rangle$ is the convolution of the spectral functions of H_S and H_B. Explicitly,

$$A(\omega)=\sum_\alpha |\langle\alpha|\psi_S\rangle|^2 A_B(\omega-\epsilon_\alpha), \tag{30}$$

where the sum is over eigenstates $|\alpha\rangle$ with eigenvalue ϵ_α of H_S, and $A_B(\omega)=\langle\psi_B|\delta(\omega-H_B)|\psi_B\rangle$. To evaluate this expression, we must diagonalize H_S in advance, to obtain its eigenvalues and eigenstates. It is, therefore, difficult to use Eq. (30) for even moderately complicated H_S. Within CSM, we calculate $A(\omega)$ without diagonalization of H_S. The convolution in Eq. (30) is implicitly performed in the course of the Chebyshev iteration. This feature is essential for all situations where system and bath degrees of freedom evolve in parallel.

We want to illustrate this point for the Hamiltonian

$$H_S=-\sqrt{\epsilon_p\omega_0}(b^\dagger+b)c^\dagger c+\omega_0 b^\dagger b \tag{31}$$

of a bosonic site, the independent boson model.[14] It is a simple model for electron-phonon coupling of localized electrons, if the bosons ($b^\dagger$) parametrize the elongation of an ion that produces an electric field which shifts the energy of an electron at the site ($c^\dagger$). The ground state of the bosonic part of H_S in the presence of a fermion, to energy $E_0=-\epsilon_p$, is the coherent state

$$|\mathrm{coh}\rangle=e^{-g^2/2}\sum_{n=0}^{\infty}\frac{g^n}{n!}(b^\dagger)^n|\mathrm{vac}\rangle,\quad g=(\epsilon_p/\omega_0)^{1/2}. \tag{32}$$

For $A_B(\omega)$, we assume a semicircular spectral function as in Eq. (25), and prepare the system in the state $|\psi\rangle=|\mathrm{coh}\rangle\otimes c^\dagger|\mathrm{vac}\rangle$. We calculate the spectral function

$$A(\omega)=\langle\psi|c^\dagger d\,\delta(\omega-H+E_0)d^\dagger c|\psi\rangle. \tag{33}$$

Physically, this corresponds to a sudden excitation of the electron from the bosonic site (c orbital) to a continuum of states given by H_B, which is related to x-ray absorption of a localized electron.[14] We know that we should obtain $A(\omega)$ as a sum of semicircular spectral functions shifted by multiples of ω_0, weighted with the Poissonian distribution of bosons in $|\mathrm{coh}\rangle$. The lowest band is centered at ϵ_p, which is the energy to remove the electron from the bosonic site. In Fig. 7, we show $A(\omega)$ calculated by CSM. The numerical result perfectly agrees with the expected outcome.

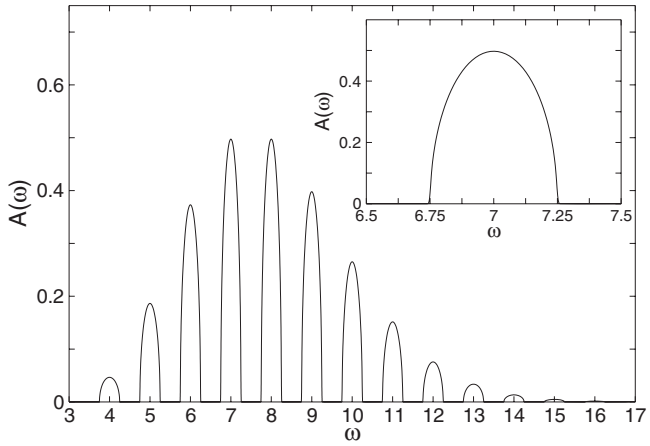

FIG. 7. Spectral function $A(\omega)$ from Eq. (33), for $\omega_0=1$, $\epsilon_p=4$ in Eq. (31), and $W=0.5$ in Eq. (25). We use $N=2^{13}$ moments and $M=2^8$ bath moments. For maximally $n_b=25$ bosons in the calculation, the scaling of H and H_B is $r/p\leqslant W/(n_b\omega_0)=0.02$. According to Sec. V, it is sufficient to use about $M=160$ bath moments. The inset displays in magnification, how accurately the semicircular spectral function is resolved for a single subband.

VIII. BOSONIC SITE COUPLED TO A BATH

We assumed in the previous section that $H_L=0$, so that system and bath degrees of freedom do not mix. Nothing changes to the applicability of our approach if this restriction is abandoned, as the next examples show. In contrast, the calculation of such "mixed" dynamics is the intended application of CSM.

Let us combine the example from the previous section with the example from Sec. IV. We get the Hamiltonian

$$H=-\Delta c^\dagger c-\sqrt{\epsilon_p\omega_0}(b^\dagger+b)c^\dagger c+\omega_0 b^\dagger b-t(d^\dagger c+c^\dagger d)+H_\mathrm{B} \tag{34}$$

of a bosonic impurity (c orbital) coupled to a fermionic bath, e.g., a lattice. Note that the impurity site is coupled to the bath via a term $H_L=-t(d^\dagger c+c^\dagger d)$ as in Eq. (6) or Eq. (28). We could also study a model with an bosonic impurity embedded in a host similar to Eq. (18), but the present form is convenient for the study of the Holstein model (Sec. VIII A).

For $\Delta<0$, the impurity is repulsive and acts as a static barrier for electron motion. Two competing mechanism determine the ground state: On the one hand, the energy of the impurity state is increased by $-\Delta$, favoring a delocalized ground state. On the other hand, the formation of a localized polaron at the bosonic impurity lowers the energy of the electron roughly by ϵ_p. A localized impurity state occurs if the loss in kinetic energy is overcome by the gain in potential energy. We know from Sec. IV that this happens—for an attractive impurity—if Δ is larger than a critical Δ_c. By a rough estimate, we expect here a localized ground state for $\epsilon_p\gtrsim\Delta_c-\Delta$.

To address this issue, we must calculate the ground state of the model (34). In Sec. IV B, we explained how to determine the ground state energy E_0 using Chebyshev expansions, testing for the divergence of Chebyshev moments for different scalings of H. This time we must obtain the ground state itself, not just its energy, to be able to calculate correlation functions for the degrees of freedom of the bosonic site. To calculate the ground state, we use the Lanczos algorithm. This requires our ability to perform two operations: To

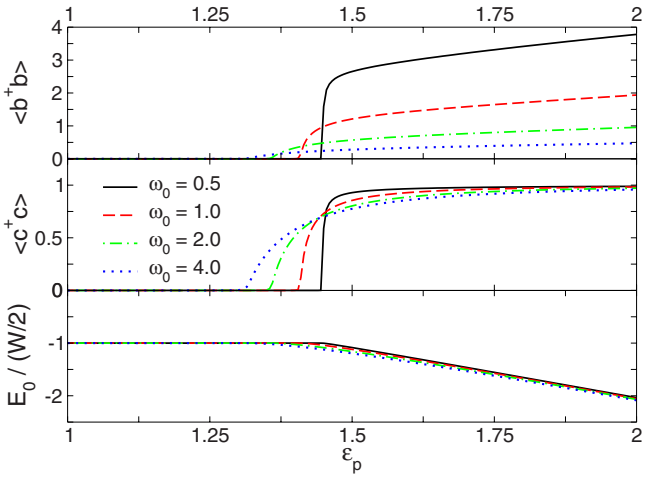

FIG. 8. (Color online) Average number of bosons $\langle b^\dagger b\rangle$, occupation probability of the impurity site $\langle c^\dagger c\rangle$, and ground state energy E_0 in dependence on ϵ_p, for the model (34) with $\Delta/W=-1$ and a semicircular $A_B(\omega)$ with $W=1$ according to Eq. (25). Calculations have been performed with Lanczos/CS for $M=2^9$ bath moments. Already $M=2^6$ moments produce accurate results away from the phase transition. Close to the phase transition, we can increase the accuracy easily by increasing M. Note that M does not need to exceed the number of Lanczos iterations.

apply H to a vector, and to calculate the scalar product between vectors. For H_B defined on the CS $\mathcal{H}_c$, Eq. (15) defines the application of H_B to a vector, and Eq. (14) [or Eq. (C3) in Appendix C] gives the scalar product. Note that for a successful application of Lanczos the moments μ_n^B should be modified by attenuation factors [Eq. (A5)], see Appendixes A and C.

In Fig. 8, we show the ground state energy E_0, the occupation probability $\langle c^\dagger c\rangle$, and the average number of bosons $\langle b^\dagger b\rangle$ calculated with the Lanczos algorithm and the CS. As in Sec. IV B, the computational effort is independent of the dimension. We used a semicircular $A_B(\omega)$ here; for a 3D lattice, the results are qualitatively the same. While E_0 is a smooth function of ϵ_p, $\langle c^\dagger c\rangle$ and $\langle b^\dagger b\rangle$ signal the phase transition from a delocalized electron to a localized polaron at a critical ϵ_p^c. For $\omega_0\to\infty$, ϵ_p^c converges to the value $\Delta_c-\Delta$ of the simple estimate. For $\omega_0\to 0$, the phase transition becomes more pronounced, as a precursor of the first-order transition in the adiabatic limit $\omega_0=0$. Note that in contrast to the (Holstein) polaron problem, this model has a phase transition also for finite ω_0.

It is perhaps surprising that the Lanczos algorithm, which constructs an orthonormal basis, works in combination with the CS construction, which is based on nonorthogonal vectors. For $H=H_B$, the Lanczos algorithm constructs an orthonormal basis of $\mathcal{H}_c$ and is equivalent to Gram-Schmidt orthonormalization of the Chebyshev vectors $|n\rangle$. It is known that the Gram-Schmidt procedure is prone to instabilities, namely, loss of orthogonality. The same is true for the Lanczos algorithm, which is a problem for the calculation of spectral functions. The calculation of the ground state, however, does not require to construct an orthonormal basis of $\mathcal{H}_c$, and loss of orthogonality is not a severe problem. For the model (18) and (34), we can force the Lanczos algorithm to fail, if $\Delta=\epsilon_p=0$ and $\omega_{\min}^B \ll -W/2$ for the lower bound $\omega_{\min}^B$ of I_B. For these parameters, the ground state is a linear combination of Chebyshev vectors $|n\rangle$ with energy $E_0>\omega_{\min}^B$, and the Lanczos algorithm will not converge. Remember also the discussion in Sec. IV B concerning the calculation of $E_0(\Delta)$ for a single fermion, where we noted that we must guarantee $E_0<\omega_{\min}^B$. In practice, we never encountered a problem with the Lanczos algorithm in combination with the CS construction. For Fig. 8, Lanczos converges fastest for large ϵ_p, when the ground state is localized at the impurity site.

A. Holstein model

The solution of the model (34) is related to the self-consistent solution of the Holstein model within DMFT. The Holstein model[15] is a standard model for electron-phonon coupling. Its Hamiltonian

$$H=-t_{ij}\sum_{ij} c_i^\dagger c_j-\sqrt{\epsilon_p\omega_0}\sum_i (b_i^\dagger+b_i)c_i^\dagger c_i+\omega_0\sum_i b_i^\dagger b_i \tag{35}$$

contains a local coupling of the electron density $(c_i^\dagger c_i)$ to dispersionless optical phonons $(b_i^\dagger)$, in addition to the kinetic energy of electrons modeled by the hopping term, and the kinetic energy of phonons with frequency ω_0. The polaron shift ϵ_p is the ground state energy of the model for $t_{ij}\equiv 0$ (see Sec. VII).

The solution of the Holstein model, especially for spectral properties, is still a demanding problem (for a recent review, see Ref. 16). We successfully used Chebyshev expansions to obtain spectral functions or the optical conductivity for finite systems.[17,18] Here, we use DMFT to relate the Holstein model to the model (34) where a coupling to a bath occurs.

Within DMFT, the (k integrated) spectral function

$$A(\omega)=\langle \mathrm{vac}|c_i\delta(\omega-H)c_i^\dagger|\mathrm{vac}\rangle \tag{36}$$

is obtained as the self-consistent solution of an impurity model with a single interacting site.[9] For the Holstein model (35), the impurity model is just the model of a single bosonic site (34) for $\Delta=0$. If we assume a semicircular density of states for the noninteracting problem, i.e., $A(\omega)$ has the functional dependence of Eq. (25) for $\epsilon_p=0$, self-consistency is established by $A(\omega)=A_B(\omega)$. For a different noninteracting density of states, this relation is more complicated, but the difference is not relevant in our context. We have shown in Sec. VI how a self-consistent calculation is performed. The complicated part of the DMFT calculation, to obtain $A(\omega)$ for the Hamiltonian (34) to given $A_B(\omega)$, is solved by an application of CSM.

In Fig. 9, we show $A(\omega)$ for two sets of parameters. For $\epsilon_p/W=0.75$, a polaron has formed as a new quasiparticle, which results in several separated bands in $A(\omega)$. We also show the imaginary part of the DMFT self-energy $\Sigma(\omega)$. In our example, it can be obtained in the form of a Green function

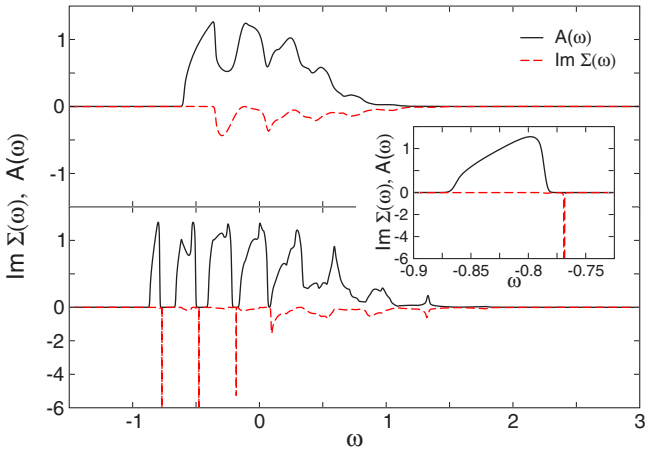

FIG. 9. (Color online) Spectral function $A(\omega)$ and imaginary part of the self-energy for the Holstein model (35) within DMFT, for a semicircular noninteracting density of states with $W=1$ [Eq. (25)]. Calculations were performed for $M=2^{11}$ bath moments. The phonon frequency is $\omega_0/W=0.25$, the coupling strength $\epsilon_p/W=0.25$ (upper panel) and $\epsilon_p/W=0.75$ (lower panel). Note the different scales for Im $\Sigma(\omega)$ in the lower panel, where a pole of $\Sigma(\omega)$ separates the lowest band. The inset displays a magnification of the lowest polaron band and the pole.

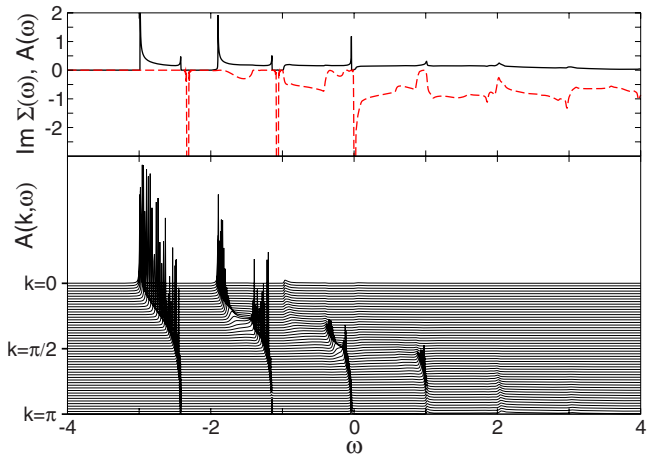

FIG. 10. (Color online) Spectral function $A(\omega)$ for the Holstein model on a 1D chain ($W=4t$ with $t=1$) within DMFT approximation, for $\omega_0/W=0.25$, $\epsilon_p/W=0.5$. The lower panel shows the k-resolved spectral function $A(k,\omega)=A^0(k,\omega-\Sigma(\omega))$, where $A^0(k,\omega)=\delta(\omega-\epsilon_k)$ with $\epsilon_k=-2t\cos k$ is the spectral function of a 1D tight-binding chain, and $\Sigma(\omega)$ the DMFT self-energy [Eq. (37)]. Calculations were performed for $M=2^{11}$ bath moments.

$$\Sigma(\omega)=\langle \mathrm{vac}|cb(\omega-H_1)^{-1}b^\dagger c^\dagger|\mathrm{vac}\rangle, \tag{37}$$

where $H_1=(1-P_0)H(1-P_0)$ is projected onto the subspace orthogonal to the boson vacuum $|\mathrm{vac}\rangle$, i.e., $P_0=|\mathrm{vac}\rangle\langle\mathrm{vac}|$. The projection guarantees that only irreducible diagrams contribute to $\Sigma(\omega)$. We calculate $\Sigma(\omega)$ once $A(\omega)$ is converged. When a polaron has formed, the polaron bands are separated by a pole in $\Sigma(\omega)$. Similar to Fig. 4, a pole close to a band has to be resolved, which requires high resolution. Note that Im $\Sigma(\omega)$ is zero for the lowest polaron band, where emission of a virtual phonon is energetically forbidden.

In Fig. 10, we show a calculation for a 1D chain. Since DMFT is constructed in the limit of high dimension, only the basic features of polaron formation in 1D are correctly described. With CSM, this calculation could be extended to a cluster of bosonic sites, using one of the recently developed cluster extensions[19] of DMFT.

B. Comparison to the analytical solution

For the Hamiltonian (34), hence for the DMFT solution of the Holstein model (35), an explicit solution for the spectral function $A(\omega)$ can be obtained as a continued fraction[20,21] (CF)

$$A(\omega)=\cfrac{1}{\omega-t^2A_B(\omega)-\cfrac{\epsilon_p\omega_0}{\omega-\omega_0-t^2A_B(\omega-\omega_0)-\cfrac{2\epsilon_p\omega_0}{\cdots}}}. \tag{38}$$

We can construct the CF from a formal Lanczos recursion. The recursion starts with the state $c^\dagger|\mathrm{vac}\rangle$ and consecutively produces the states $(b^\dagger/\sqrt{n!})c^\dagger|\mathrm{vac}\rangle$, which form an orthonormal basis of the Hilbert space $\mathcal{H}_S$ of the bosonic impurity site. In this basis, the matrix of H [Eq. (34)] is tridiagonal, and $A(\omega)$, which is the (1,1) element of this matrix, can be expressed as a CF.

To treat the coupling to the bath in Eq. (34), we use Eq. (30). If the electron is in the bath, the states of the bosonic site evolve by the Hamiltonian $H_S'=\omega_0 b^\dagger b$. In the nth level of the CF (38), which corresponds to the excitation of n bosons, we must, therefore, insert $A_B(\omega)$ with energy shift $A_B(\omega-n\omega_0)$.

For this example, the (Lanczos) recursion leading to the CF creates every eigenstate of $\omega_0 b^\dagger b$ one by one. Otherwise, if eigenstates were mixed during the recursion, linear combinations $\Sigma_n w_n A_B(\omega-n\omega_0)$ would occur instead of $A_B(\omega-n\omega_0)$. The weight w_n had to be determined during the recursion and depended on the parameters. This is one of the many obstructions that prohibit a generalization of Eq. (38) to other models, e.g., with a cluster of interacting (bosonic) sites or different electron-phonon coupling. Within CSM, these consideration are pointless, as its application does not rely on our ability to solve one part of the Hamiltonian prior to the actual calculation. Note also that the general CS construction allows to calculate the ground state and correlation functions that cannot be expressed in a form such as Eq. (38).

IX. TIME EVOLUTION OF A WAVE PACKET ON A CHAIN COUPLED TO LEADS

In the preceding sections, we used the CS construction for the calculation of spectral properties within CSM. It is an essential advantage of Chebyshev techniques, and the CS construction, that they can be easily adapted to new problems. In this section, we treat the time evolution of a wave packet on a chain coupled to leads. To describe the coupling

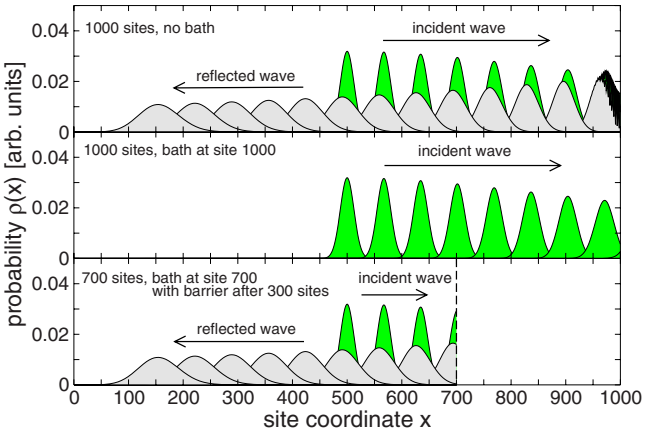

FIG. 11. (Color online) Time evolution of a Gaussian wave packet Eq. (41), with $2\sigma^2=25^2$ and $K=1$. The time step between two curves is $\delta t=40$. The group velocity of the wave packet is given by the dispersion $\epsilon_k=-2t_{\text{hop}}\cos k$ as $v=(\partial\epsilon_k/\partial k)|_K$. Per time step, the wave packet moves $v\times\delta t\approx 67$ lattice sites. The three panels correspond to the situations described in the text.

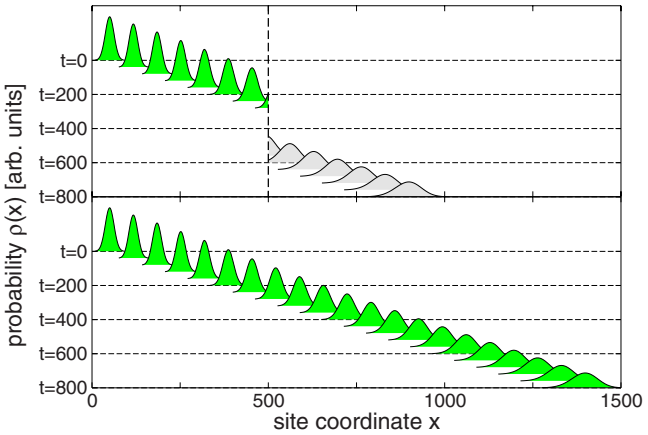

FIG. 12. (Color online) Time evolution of a Gaussian wave packet with same parameters as in Fig. 11. Time is shown on the vertical axis. A bath which mimics a chain segment of 500 sites is placed between sites 500 and 501 of the chain (vertical dashed line). The wave enters the bath and reemerges after a delay $\Delta t=500/v\approx 300$ (upper panel). After transmission through the bath, the wave packet is 500 sites behind the wave packet on a simple chain, whose propagation is shown in the lower panel for comparison.

to a lead, we can use the CS construction from Sec. III without change.

Within Chebyshev techniques, time evolution of a vector $|\psi(t)\rangle=e^{-iHt}|\psi(0)\rangle$ is determined from the Chebyshev expansion of the time evolution operator[22]

$$e^{-iHt}=c_0+2\sum_{n=1}^{\infty}c_nT_n(H). \tag{39}$$

The expansion coefficients are given by Bessel functions

$$c_n=\int_{-1}^{1}\frac{T_n(x)e^{-ixt}}{\pi\sqrt{1-x^2}}=(-i)^nJ_n(t), \tag{40}$$

where $J_n(t)$ denotes the Bessel function of order n. As usual, we omit the scaling of H. Since $J_n(t)$ decays rapidly for $n\gg t$, the infinite series can be truncated to obtain $|\psi(t)\rangle$ with high precision. An adequate choice for the number of moments is given by $N\gtrsim 1.5t$.

We apply the Chebyshev time evolution to the propagation of an electron along a chain of length L, which is coupled to a bath at site L. The chain geometry is identical to the example studied in Sec. VI, and the Hamiltonian is given by Eq. (28). The calculation of $T_n(H)|\psi(0)\rangle$ proceeds along the lines established in previous sections, and $|\psi(t)\rangle$ is obtained from Eqs. (39) and (40).

At $t=0$, we place a Gaussian wave packet of width σ and momentum K centered at site $m_0=L/2$,

$$|\psi(0)\rangle\propto\sum_m e^{iKm}e^{-(m-m_0)^2/2\sigma^2}c_m^\dagger|\text{vac}\rangle \tag{41}$$

(we omit normalization here), and let it evolve in time (see Fig. 11). Without a bath, the particle is reflected at the right end of the chain and returns, moving to the left.

We now add a bath to the right end, whose spectral function $A_B(\omega)$ is given by Eq. (25), with $W=4t$. Since this is the spectral function of a half-infinite chain at its open end, also the full Hamiltonian H describes a half-infinite chain. Physically, the open boundary at site L is removed by coupling to an infinite lead. In contrast to the previous situation, the particle will not be reflected at site L, but propagates into the bath (or lead). As the middle panel in Fig. 11 shows, no spurious reflection occurs.

In the Hamiltonian H, sites $1\ldots L$ are explicitly included while sites $\geqslant L+1$ of the lead are realized through the bath. In this way, we can use our Chebyshev approach to realize "transparent boundary conditions"[23,24] that mimic an infinite system with a finite number of lattice sites explicitly treated. Transparent boundary conditions are implemented in Refs. 23 and 24 by a modification of time propagation algorithms, e.g., Crank-Nicholson. Within the CS construction, modified boundary conditions are implemented independently of the actual calculation. For time propagation, we use the same Eqs. (14)–(16) as for the calculation of spectral properties. This permits us to use a variety of algorithms, like we used Lanczos algorithm in Sec. VIII. We could also use the CS in combination with Crank-Nicholson, but for the time-independent Hamiltonians considered here Chebyshev time propagation is most efficient.

Transparent boundary conditions correspond to a particular choice for $A_B(\omega)$. We have the freedom to choose any $A_B(\omega)$. For example, if $A_B(\omega)$ is the spectral function of a 300 site chain at its end, and $L=700$, H describes a chain of length $L+300=1000$. As before, the particle is reflected and returns moving to the left (see bottom panel in Fig. 11 in comparison with the top panel). The point is that the reflecting barrier is now realized through a bath with carefully chosen $A_B(\omega)$, and not by lattice sites $701\ldots L$ explicitly included in the Hamiltonian. We might call these "reflecting boundary conditions.":

For Fig. 12, we slice the chain in two parts which are connected by a bath. Similar to the previous example, the

bath shall replace a finite segment of the chain. Since the bath has now two entry points—at its junction to the left and to the right part of the chain—this example involves off-diagonal bath spectral functions. Let $d_{1/2}^{(\dagger)}$ denote the operators to the two entry points. Following Sec. III, we need two different types of Chebyshev vectors $|n_b\rangle = T_n(H_B) d_b^\dagger |\mathrm{vac}\rangle$ for $b=1,2$. Equation (16) generalizes to $d_a |n_b\rangle = \mu_n^{B,ab} |\mathrm{vac}\rangle$, where the four different types of moments $\mu_n^{B,ab}$ correspond to the four different spectral functions characterizing the bath: the diagonal $A_{11}^B(\omega)$, $A_{22}^B(\omega)$ for moving into the bath and back, and the off-diagonal $A_{12}^B(\omega)$, $A_{21}^B(\omega)$ for moving through the bath. The latter ones give the energy-dependent transmission rate through the bath. Only for nonzero $A_{12}^B(\omega)$, $A_{21}^B(\omega)$, the bath connects the two parts of the chain. In Fig. 12, the spectral functions of the bath are these of a finite chain segment. We see how the wave moves into the bath at its left side, passes through and reemerges at the right site. The bath perfectly mimics the transmission through a chain segment. As we noted above, we have the freedom to change the behavior by a different choice of the bath spectral functions $A_{ab}^B(\omega)$.

X. SUMMARY AND OUTLOOK

In this paper, we introduced the Chebyshev space method (CSM) for the treatment of degrees of freedom with nontrivial dynamics. In our examples, the degree of freedom is given by the operator $d^\dagger$ which creates a fermion in a bath, and the dynamics of $d^\dagger$ is specified by a spectral function $A_B(\omega)$. We demonstrated for various examples, how CSM yields extremely accurate results with modest computational effort. For the example in Secs. IV B and VIII, the computational effort is even independent of the geometry or dimension.

A particular advantage of the Chebyshev space (CS) construction is that it still provides a Hamiltonian H_B acting on a Hilbert space, albeit it is an abstract space without a direct physical counterpart. We can use this form of H_B in different situations, such as in the Lanczos algorithm or for time propagation. We have, therefore, obtained a numerically exact Hamiltonian treatment of degrees of freedom with nontrivial dynamics, which does not rely on a discretization of spectral functions.

The concept of a CS and an ancillary Hamiltonian H_B acting on this space is very general. It makes no assumption about the Hamiltonian H_S for the quantum system, and can be extended to various problems mentioned in the Introduction. We have obtained preliminary results for the Holstein model within cluster extensions of DMFT, but the issue needs further exploration from the physical point of view.

An especially important topic is the extension to interacting fermions at finite density or to bosonic baths. With a single fermion, the bath is in the vacuum state $|\mathrm{vac}\rangle$ if the fermion is removed by application of the operator d. This simplification is no longer true for finite fermion density, when adding and removing a fermion create particle-hole pairs in the bath, which initially was prepared as the particle-hole vacuum (or Fermi sea). We have derived a formalism that deals with particle-hole pairs in the context of CSM. The CS construction is used in this formalism without change. A similar formalism for bosonic baths can be derived. As a first result, this formalism allows for the calculation of the core level spectral function in the x-ray absorption problem.[14] The spectral function can be calculated exactly in this case. It is equivalent to the Anderson model with one immobile spin species, but the extension to the full Kondo problem is much harder. The presentation of this formalism is left for a future publication.

The CS construction can be also used in the context of (diagrammatic) Green function techniques. Any Feynman diagram contains energy-dependent Green functions which represent a degree of freedom with nontrivial dynamics. The difficult task is to sum up a huge number of Feynman diagrams. Note that we can interpret the self-consistent calculation of the Holstein model in Sec. VIII A as the exact summation of a certain class of Feynman diagrams. The bosonic impurity model defines a set of skeleton diagrams for this problem, and imposing self-consistency corresponds to replacing bare Green functions ("thin lines" in a diagram) by renormalized Green functions ("thick lines"). In this example, diagrams are selected by a geometric rule, but with some modifications a different selection rule can be implemented. The CSM provides the link between exact numerical techniques for Hamilton operators and general approximation schemes for Green functions.

In conclusion, we believe that the CSM introduced in this work is a powerful addition to existing numerical techniques in theoretical physics or chemistry. It substantially enlarges the field of applications of Chebyshev techniques and keeps their advantages. The results we obtained in this work are promising for successful applications to more complicated problems, and the possible combination of CSM with other techniques shall prove fruitful. The further development of CSM and its application to the study of physical problems mentioned in the introduction are the subject of current research.

ACKNOWLEDGMENT

We are indebted to G. Wellein for helpful comments during the preparation of this paper.

APPENDIX A: CHEBYSHEV EXPANSIONS AND THE KERNEL POLYNOMIAL

In this paper, we repeatedly approximate a function $f:[-1,1]\to\mathbb{R}$ by a finite Chebyshev series

$$f_N(x) = \frac{1}{\pi\sqrt{1-x^2}}\left[\mu_0 + 2\sum_{n=1}^{N-1}\mu_n T_n(x)\right], \tag{A1}$$

where the moments μ_n are given by

$$\mu_n = \int_{-1}^{1} f(x) T_n(x) dx. \tag{A2}$$

A central question is how good $f(x)$ is approximated by f_N. Functional analysis teaches us that the f_N converge to f in the integral norm

$$\|f(x) - f_N(x)\| = \left[\int_{-1}^{1} \frac{[f(x) - f_N(x)]^2}{\pi\sqrt{1-x^2}} dx \right]^{1/2}, \quad \text{(A3)}$$

corresponding to the scalar product used in Eq. (2), provided $\|f(x)\|$ is finite. For practical purposes, this convergence property is too weak, and we demand uniform or at least pointwise convergence. We do not try to resolve the issue of convergence here, but state that for sufficiently smooth $f(x)$ the series f_N will converge uniformly to f on any closed subinterval of $[-1,1]$ that excludes the endpoints ± 1. Convergence at the end points is of course spoiled by the divergence of the weighting function $(1-x^2)^{-1/2}$.

In physical applications, we want to expand spectral functions which are not necessarily continuous, and perhaps contain some δ peaks due to (quasi-) particle states with infinite lifetime. In this case, the series cannot converge uniformly—otherwise its limit f had to be continuous itself—but the situation is even worse. The infamous Gibbs phenomenon ruins convergence at all: In plain words, the series (A1) fails to converge in the vicinity of a discontinuity, e.g., a jump of the function, instead shows rapid oscillations whose height does not decrease as the number of terms $N \to \infty$. The Gibbs phenomenon is a severe obstacle for practical applications.

Fortunately, the problem arising from the Gibbs phenomenon is solved for Chebyshev expansions.[1–4] It is possible to specify, prior to the calculation of the μ_n, a set of attenuation factors g_n^N, $n=0,\ldots,N-1$ for every N, such that the modified approximants

$$\tilde{f}_N = \frac{1}{\pi\sqrt{1-x^2}} \left[g_0^N \mu_0 + 2 \sum_{n=1}^{N-1} g_n^N \mu_n T_n(x) \right] \quad \text{(A4)}$$

do not show the Gibbs phenomenon but approximate a wide class of functions in a favorable way. Plainly spoken, the attenuation factors damp out high frequency oscillations that otherwise lead to spurious results in the finite series. Instead of a more precise formulation, we show an example in Fig. 13. The best choice in many cases are factors g_n^N derived from the so-called Jackson kernel,[4] leading to the explicit expression

$$g_n^N = \frac{(N-n+1)\cos\frac{\pi n}{N+1} + \sin\frac{\pi n}{N+1}\cot\frac{\pi}{N+1}}{N+1}. \quad \text{(A5)}$$

Modifying moments with these attenuation factors is related to convolution with an almost Gaussian peak of width $\sigma = \pi/N$ (see Ref. 5). An important property of the modification with these attenuation factors is that the modified approximants $\tilde{f}_N$ are positive whenever the function f is. This is not true for the unmodified approximants (see Fig. 13). Besides Eq. (A5), other suggestions for attenuation factors exist, see Ref. 5 for a different choice in the context of Green functions, with an application in Ref. 25.

Note that the factors g_n^N in Eq. (A5) have the property that $g_n^N \to 1$ for $N \to \infty$. We can, therefore, always use the attenuation factors g_n^N without losing information. For functions with discontinuities, multiplication with attenuation factors enforces the decay of moments relevant for good approximation properties. For smooth $f(x)$, the moments itself decay rapidly, and multiplication with the attenuation factors does not change the result for not too small N.

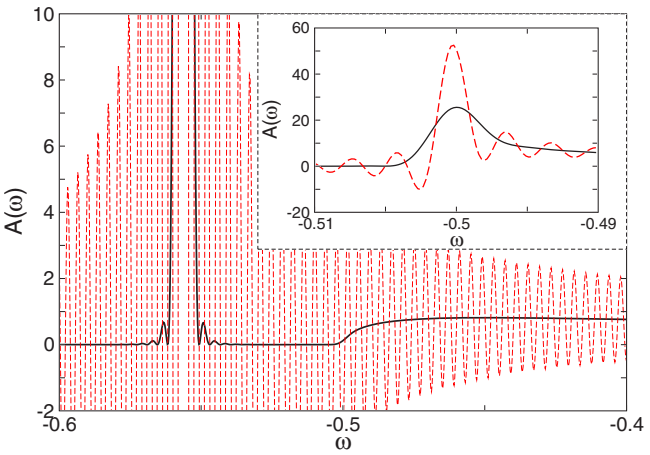

FIG. 13. (Color online) Shown is the spectral function to the Hamiltonian (18) and $\Delta=0.4$. The solid curve is calculated with attenuation factors from Eq. (A5) and is identical to the curve in Fig. 4. The dashed curve is calculated without attenuation factors. The inset displays the curve from Fig. 4 to $\Delta=0.26$ and $N=2^{10}$, again with (solid) and without (dashed) attenuation factors. These two curves illustrate the remark from the text: After multiplication with attenuation factors the reconstructed spectral function seems to be smooth. However, the unmodified moments correspond to a discontinuous spectral function with a pole close to $\omega=-0.5$. The slow decay of moments of this spectral function results in oscillations. The pole is resolved only by increasing N and keeping the attenuation factors (see the curves in Fig. 4 up to $N=2^{16}$).

The introduction of attenuation factors is the essence of the kernel polynomial method (KPM). Within KPM, resolution for spectral functions is already obtained with a fairly small number of moments, thus allowing for accurate calculations with moderate demands on computational time or memory. The possible resolution is much better than known, e.g., from the Lanczos algorithm where peaks are commonly broadened by a Lorentzian function. Furthermore, the resolution of the Chebyshev expansion is uniform over the energy interval, and does not deteriorate toward the center of the spectrum.

APPENDIX B: DETERMINANTS AND TWO-TERM RECURRENCES

We formulate a well-known determinant identity related to two-term recurrences. Define, for each n and given a_j, b_j, c_j, a tridiagonal $n \times n$ matrix

$$A_n = \begin{pmatrix} a_1 & c_1 & & & & & \\ b_1 & a_2 & c_2 & & & & \\ & b_2 & a_3 & \ddots & & & \\ & & \ddots & \ddots & \ddots & & \\ & & & \ddots & a_{n-2} & c_{n-2} & \\ & & & & b_{n-2} & a_{n-1} & c_{n-1} \\ & & & & & b_{n-1} & a_n \end{pmatrix}. \quad \text{(B1)}$$

Expanding in the last row yields

$$\det A_n = a_n \det A_{n-1} - b_{n-1}c_{n-1} \det A_{n-2}. \tag{B2}$$

From this relation, it follows that the characteristic polynomials $\chi_n = \det(x - A_n)$ obey the two-term recurrence

$$\chi_0 = 1, \quad \chi_1 = x - a_1,$$

$$\chi_{n+1} = (x - a_{n+1})\chi_n - b_n c_n \chi_{n-1}. \tag{B3}$$

Conversely, for polynomials P_n defined by a two-term recurrence

$$P_0 = 1, \quad P_1 = a_1 x, \quad P_n = a_n x P_{n-1} - b_{n-1} P_{n-2}, \tag{B4}$$

this result implies that

$$P_n = \det \begin{pmatrix} a_1 x & d_1 & & & \\ c_1 & a_2 x & d_2 & & \\ & c_2 & a_3 x & d_3 & \\ & & c_3 & a_4 x & \\ & & & & \ddots \end{pmatrix}, \tag{B5}$$

where c_n, d_n is chosen in such a way that $c_n d_n = b_n$, e.g., for positive b_n we may choose $c_n = d_n = \sqrt{b_n}$. By multiplying the jth column—or equivalently, jth row—by $1/a_j$, P_n can be expressed as the characteristic polynomial of a tridiagonal matrix times a prefactor $\Pi_{j=1}^{n} a_j$.

In particular, the Chebyshev polynomials fulfill

$$T_n(x) = \det \begin{pmatrix} x & 1 & & & \\ 1 & 2x & 1 & & \\ & 1 & 2x & 1 & \\ & & 1 & 2x & \\ & & & & \ddots \end{pmatrix}. \tag{B6}$$

Multiplying the second to the last column by $1/2$, we find the result $T_M(x) = 2^{M-1} \det(x - H_B^M)$ used in the main text.

APPENDIX C: HERMITICITY OF H_B

We first prove that H_B is Hermitian by calculating explicitly that H_B is equal to its adjoint. The product of two Chebyshev polynomials satisfies the identity[10]

$$T_m(x)T_n(x) = [T_{m+n}(x) + T_{m-n}(x)]/2. \tag{C1}$$

For notational convenience, we define here $T_{-n}(x) = T_n(x)$. It follows for Chebyshev vectors $|n\rangle = T_n(H_B)|0\rangle$ that

$$\langle m|n\rangle = (\mu^B_{m+n} + \mu^B_{m-n})/2, \tag{C2}$$

where we again define $\mu^B_{-n} = \mu^B_n$. The scalar product of two vectors $|a\rangle = \sum_{n=0}^{\infty} a_n |n\rangle$, $|b\rangle = \sum_{n=0}^{\infty} b_n |n\rangle$ given as linear combinations of Chebyshev vectors, is now found as

$$\langle b|a\rangle = \sum_{m,n=0}^{\infty} b_m^* a_n (\mu^B_{m+n} + \mu^B_{m-n})/2. \tag{C3}$$

Since $\mu^B_{m-n} = \mu^B_{n-m}$, with the notational convention adopted above, we have $\langle a|b\rangle = \langle b|a\rangle^*$, as it must be (note that the moments are real).

To calculate a scalar product with H_B, we use that

$$H_B|a\rangle = \frac{1}{2}\sum_{n=0}^{\infty} a_n(|n-1\rangle + |n+1\rangle), \tag{C4}$$

where the summand for $n=0$ is $a_0(|-1\rangle + |1\rangle)/2 = a_0|1\rangle$ in accordance with Eq. (26). Inserting this equation, we find

$$\langle b|H_B|a\rangle = \frac{1}{2}\sum_{m,n=0}^{\infty} b_m^* a_n (\langle m|n-1\rangle + \langle m|n+1\rangle)$$

$$= \frac{1}{4}\sum_{m,n=0}^{\infty} b_m^* a_n (\mu^B_{m+n-1} + \mu^B_{m-n+1} + \mu^B_{m+n+1} + \mu^B_{m-n-1}). \tag{C5}$$

We can condense this equation to matrix-vector form

$$\langle b|H_B|a\rangle = \frac{1}{4}\sum_{m,n=0}^{\infty} b_m^* a_n M_{mn},$$

$$M_{mn} = \mu^B_{m+n-1} + \mu^B_{m-n+1} + \mu^B_{m+n+1} + \mu^B_{m-n-1}. \tag{C6}$$

Since M_{mn} depends only on the sum and difference of m, n, $M_{mn} = M_{nm} = M^*_{nm}$ (the moments are real, and $\mu^B_{-l} = \mu^B_l$). It follows that $\langle b|H_B|a\rangle = \langle a|H_B|b\rangle^*$, and H_B is Hermitian.

We derived the hermiticity of H_B without imposing any constraint on the moments. This may be a bit puzzling, because the moments should correspond to a non-negative spectral function $A_B(\omega)$ if H_B is Hermitian. The puzzle is resolved by observing that the scalar product (C3) has to be positive (semi) definite. This requirement imposes constraints on the moments that are equivalent to a non-negative $A_B(\omega)$. To mention one, $\langle n|n\rangle = (\mu^B_0 + \mu^B_{2n})/2$, so it must $\mu^B_{2n} \geqslant -\mu^B_0$. Consider, for example, $H_B = 0$, equivalent to $A_B(\omega) = \delta(\omega)$. We then have $\mu^B_{2n} = (-1)^n$, $\mu^B_{2n+1} = 0$, i.e., equality holds in this inequality. The scalar product (C3) is positive semidefinite, but not positive definite, as $|n\rangle = 0$ and $\langle n|n\rangle = 0$ for odd n.

We can characterize the properties of the scalar product (C3) better, if we consider Chebyshev expansions

$$f(x) = \sum_{m=0}^{\infty} f_m T_m(x), \quad g(x) = \sum_{m=0}^{\infty} g_m T_m(x) \tag{C7}$$

of functions $f, g : [-1, 1] \to \mathbb{R}$, and the associated vectors

$$|f\rangle = \sum_{m=0}^{\infty} f_m |m\rangle, \quad |g\rangle = \sum_{m=0}^{\infty} g_m |m\rangle \tag{C8}$$

in $\mathcal{H}_c$. With Eqs. (C1) and (5), we find for $A_B(\omega)$ as in Eq. (4) $\int_{-1}^{1} T_m(x)T_n(x)A_B(x)dx = (\mu^B_{m+n} + \mu^B_{m-n})/2$, which implies

$$\int_{-1}^{1} f(x)g(x)A_B(x)dx = \langle f|g\rangle. \tag{C9}$$

The scalar product (C3) in $\mathcal{H}_c$, therefore, corresponds to a scalar product of functions $[-1, 1] \to \mathbb{R}$, given as the integral on the left hand side of this equation. We conclude that for continuous $A_B(\omega)$ the scalar product (C3) is positive

semidefinite (positive definite) if and only if $A_B(\omega) \geqslant 0$ [and $A_B(\omega)$ does not vanish on an open interval].

We discussed in Appendix A that a truncated, finite Chebyshev expansion of $A_B(\omega)$ may fail to be positive although $A_B(\omega)$ is. Positivity of the finite Chebyshev expansion is ensured by using attenuation factors of a positive kernel like in Eq. (A5). To obtain a positive definite scalar product (C3) for a finite Chebyshev expansion, we must, therefore, use modified moments $\mu_n^B g_n^M$ instead of unmodified moments μ_n^B. For the Lanczos algorithm, used in Sec. VIII, which aims at constructing an orthonormal basis in Krylov subspaces, positive definiteness of Eq. (C3) is crucial. For the calculation of spectral or dynamical properties, it is not that essential. However, we learned in Appendix A that the modification of moments by attenuation factors never ruin a result. Hence, our recommendation is to always modify the moments μ_n^B put into the calculation with attenuation factors.

APPENDIX D: EIGENSTATES OF H_B^M

According to Appendix B, the characteristic polynomial of H_B^M [Eq. (26)] is $\det[x-(H_B^M)_{mn}]=2^{-(M-1)}T_M(x)$. The Mth Chebyshev polynomial $T_M(x)=\cos(M \arccos x)$ has M distinct real roots

$$x_j = \cos\frac{\pi(j-1/2)}{M}, \quad j=1,\ldots,M. \tag{D1}$$

We concluded in Sec. V that H_B^M is diagonalizable with real eigenvalues x_j. The eigenstates of H_B^M can be given explicitly, using the recurrence (1). The state

$$|\phi_j\rangle = |0\rangle + 2\sum_{m=1}^{M-1} T_m(x_j)|m\rangle \tag{D2}$$

is the eigenstate of H_B^M to eigenvalue x_j, i.e., $H_B^M|\phi_j\rangle = x_j|\phi_j\rangle$. If we use Eq. (26) to calculate $H_B^M|\phi_j\rangle$, we find that the term proportional to $T_M(x_j)$ drops out, because x_j is a root of $T_M(x)$. This explains why the roots of $T_M(x)$ occur as eigenvalues of H_B^M.

Scalar products of the states $|\phi_j\rangle$ have to be calculated using Eq. (C3). It turns out that the $|\phi_j\rangle$ are not orthogonal to each other. Indeed, while H_B is Hermitian, the truncated H_B^M is not Hermitian. If one repeats the calculations leading to Eq. (C5), now with upper summation bound $M-1$ instead of ∞, one finds that a term $a_{M-1}|M\rangle$ is missing, and the scalar product is not symmetric in $|a\rangle, |b\rangle$. The mathematical reason that H_B^M fails to be Hermitian is that H_B^M is obtained from H_B via a nonorthogonal projection. Working with a non-Hermitian operator could in principle spoil the calculation for $M<N$. We found in Sec. V that this does not happen. By an explicit calculation of the spectral function encoded by H_B^M, we now show that the nonhermiticity of H_B^M has no (negative) consequences.

As Fig. 5 shows, for $N \gg M$, CSM resolves M poles in the spectral function encoded by H_B^M. The position of the poles is determined by x_j, and their weight w_j can be calculated using the eigenstates $|\phi_j\rangle$. We first expand the zeroth Chebyshev vector $|0\rangle$ in the $|\phi_j\rangle$. With the identity

$$\frac{1}{M}\sum_{j=1}^{M} T_m(x_j)T_n(x_j) = \begin{cases} \frac{1}{2}\delta_{mn}, & m,n \neq 0 \\ 1, & m=n=0, \end{cases} \tag{D3}$$

which is a kind of discrete orthogonality relation for Chebyshev polynomials, we find that

$$|0\rangle = \frac{1}{M}\sum_{j=1}^{M} |\phi_j\rangle. \tag{D4}$$

The coefficients in this linear combination are $T_0(x_j)=1$. Now $\delta(\omega-H_B^M)|\phi_j\rangle = \delta(\omega-x_j)|\phi_j\rangle$, and we obtain

$$\langle 0|\delta(\omega-H_B^M)|0\rangle = \sum_{j=1}^{M} w_j \delta(\omega-x_j), \tag{D5}$$

with the weight of each pole given by

$$w_j = \frac{1}{M}\langle 0|\phi_j\rangle = \frac{1}{M}\left[\mu_0^B + 2\sum_{m=1}^{M-1} T_m(x_j)\mu_m^B\right]$$
$$= \frac{\pi}{M}\sqrt{1-x_j^2}A_B(x_j). \tag{D6}$$

The first line in this equation follows from the definition (D2), and the second line from comparison with Eq. (4). Here, $A_B(\omega)$ is assumed as an expansion with M Chebyshev moments, in accordance with the truncation of H_B^M. The weight w_j of the pole at x_j is, therefore, the value of $A_B(\omega)$ at the position of the pole, weighted by the inverse $(1-x^2)^{1/2}$ of the weighting function for Chebyshev expansions (and with $1/M$ for M poles). Using the attenuation factors from Eq. (A5), $A_B(\omega)$ is positive, which implies that the weight w_j of each pole is positive. The total weight is

$$\sum_{j=1}^{M} w_j = \langle 0|\frac{1}{M}\sum_{j=1}^{M}|\phi_j\rangle = \langle 0|0\rangle = \mu_0^B = 1, \tag{D7}$$

according to the sum rule $\mu_0^B = \int_{-1}^{1} A_B(x)dx = 1$. This result also follows with the explicit expression for w_j in terms of the μ_n^B [first line of Eq. (D6)], and Eq. (D3). If we express w_j by $A_B(\omega)$ [second line of Eq. (D6)], we find a nice relation to quadrature formulas from numerical integration. In the expression for the total weight

$$\sum_{j=1}^{M} w_j = \frac{\pi}{M}\sum_{j=1}^{M}\sqrt{1-x_j^2}A_B(x_j), \tag{D8}$$

the right hand side is the formula for Gauss-Chebyshev integration[26] of a function, with abscissas at x_j. Now $A_B(\omega)$, expanded with M Chebyshev moments, is a polynomial of order M times the weighting function $(1-x^2)^{-1/2}$. The Gauss-Chebyshev integration formula is exact in this case, and we find once again $\sum_{j=1}^{M} w_j = \int_{-1}^{1} A_B(x)dx = 1$.

We can finally understand why H_B^M is non-Hermitian using the scalar product Eq. (C9). A state $|\phi_j\rangle$ corresponds to the function

$$\phi_j(x) = T_0(x_j)T_0(x) + 2\sum_{m=1}^{M-1} T_m(x_j)T_m(x), \tag{D9}$$

which is the Mth Chebyshev approximation to $\delta(x-x_j)$. With a finite number of moments, $\phi_j(x)$ has finite width. Using Eq. (C9) for the scalar product,

$$\langle \phi_j | \phi_k \rangle = \int_{-1}^{1} \phi_j(x)\phi_k(x)A_B(x)dx, \tag{D10}$$

we see that the integral is nonzero even for $j \neq k$, since the two functions $\phi_j(x)$, $\phi_k(x)$ have finite overlap. The deviation of H_B^M from hermiticity is, therefore, an effect of finite resolution of a finite Chebyshev expansion. The larger M, the smaller is the overlap and hence the scalar product. We conclude that in the limit $M \to \infty$, the states $|\phi_j\rangle$ are mutually orthogonal, in accordance with hermiticity of H_B proved in Appendix C.

We have obtained two important results in this Appendix. First, despite its nonhermiticity, H_B^M encodes a positive, normalized spectral function. Using the truncated H_B^M, as in Sec. V for $M < N$, does, therefore, not lead to erroneous results. Second, we related the CS construction for H_B to an explicit representation, Eq. (7). In particular, Eq. (D6) shows how to obtain from given moments μ_m^B a discretization [Eq. (12)] of $A_B(\omega)$ [the opposite way is given by Eq. (5)]. The point is that the CS construction indicates how to discretize a given $A_B(\omega)$ to prescribed resolution. Within CSM, we can work without a discretization anyway. The reader should note that the CS construction is no longer equivalent to the discretization of $A_B(\omega)$ in the extensions of CSM mentioned in Sec. X.

[1] R. N. Silver and H. Röder, Int. J. Mod. Phys. C **5**, 935 (1994).
[2] L.-W. Wang and A. Zunger, Phys. Rev. Lett. **73**, 1039 (1994).
[3] L.-W. Wang, Phys. Rev. B **49**, 10154 (1994).
[4] R. N. Silver, H. Röder, A. F. Voter, and D. J. Kress, J. Comput. Phys. **124**, 115 (1996).
[5] A. Weiße, G. Wellein, A. Alvermann, and H. Fehske, Rev. Mod. Phys. **78**, 275 (2006).
[6] S. Datta, *Electronic Transport in Mesoscopic Systems* (Cambridge University Press, Cambridge, 1995).
[7] D. K. Ferry and S. M. Goodnick, *Transport in Nanostructures* (Cambridge University Press, Cambridge, 1997).
[8] A. C. Hewson, *The Kondo Problem to Heavy Fermions* (Cambridge University Press, 1997).
[9] A. Georges, G. Kotliar, W. Krauth, and M. J. Rozenberg, Rev. Mod. Phys. **68**, 13 (1996).
[10] *Handbook of Mathematical Functions with Formulas, Graphs, and Mathematical Tables*, edited by M. Abramowitz and I. A. Stegun (Dover, New York, 1970).
[11] R. Haydock, V. Heine, and M. J. Kelly, J. Phys. C **5**, 2845 (1972).
[12] E. R. Gagliano and C. A. Balseiro, Phys. Rev. Lett. **59**, 2999 (1987).
[13] Q. F. Zhong, S. Sorella, and A. Parola, Phys. Rev. B **49**, 6408 (1994).
[14] G. D. Mahan, *Many-Particle Physics* (Kluwer Academic, Dordrecht/Plenum, New York, 2000).
[15] T. Holstein, Ann. Phys. (N.Y.) **8**, 343 (1959).
[16] H. Fehske and S. A. Trugman, in *Polarons in Advanced Materials*, edited by A. S. Alexandrov, Springer Series in Material Sciences Vol. 103 (Springer, Dordrecht, 2007), pp. 393–461.
[17] G. Schubert, G. Wellein, A. Weiße, A. Alvermann, and H. Fehske, Phys. Rev. B **72**, 104304 (2005).
[18] H. Fehske, A. Alvermann, M. Hohenadler, and G. Wellein, in *Polarons in Bulk Materials and Systems With Reduced Dimensionality*, edited by G. Iadonisi, J. Ranninger, and G. De Filippis, International School of Physics Enrico Fermi Vol. 161 (IOS, Amsterdam, 2006), pp. 285–296.
[19] T. Maier, M. Jarrell, T. Pruschke, and M. Hettler, Rev. Mod. Phys. **77**, 1027 (2005).
[20] S. Ciuchi, F. de Pasquale, S. Fratini, and D. Feinberg, Phys. Rev. B **56**, 4494 (1997).
[21] H. Sumi, J. Phys. Soc. Jpn. **36**, 770 (1974).
[22] H. Tal-Ezer and R. Kosloff, J. Chem. Phys. **81**, 3967 (1984).
[23] J. R. Hellums and W. R. Frensley, Phys. Rev. B **49**, 2904 (1994).
[24] C. A. Moyer, Am. J. Phys. **72**, 351 (2003).
[25] M. Hohenadler, G. Wellein, A. R. Bishop, A. Alvermann, and H. Fehske, Phys. Rev. B **73**, 245120 (2006).
[26] W. H. Press, S. A. Teukolsky, W. T. Vetterling, and B. P. Flannery, *Numerical Recipes in C: The Art of Scientific Computing*, 2nd ed. (Cambridge University Press, Cambridge, 1992).